Synthesis, Crystal Structure and Li Motion of Li8SeN2 and Li8TeN2

Daniel Bräunling, Oliver Pecher, Dmytro Trots, Anatoliy Senyshyn, Dmitry Zherebtsov, Frank Haarmann, Rainer Niewa

Zeitschrift für Anorganische und Allgemeine Chemie

Synthesis, Crystal Structure and Li Motion of Li_8SeN_2 and Li_8TeN_2

Journal:	*Zeitschrift für Anorganische und Allgemeine Chemie*
Manuscript ID:	zaac.201000002.R1
Wiley - Manuscript type:	Article
Date Submitted by the Author:	12-Feb-2010
Complete List of Authors:	Bräunling, Daniel; TU München, Chemie Pecher, Oliver; MaxPlanckInstitut für Chemische Physik fester Stoffe Trots, Dmytro; Universität Bayreuth, Bayerisches Geoinstitut Senyshyn, Anatoliy; Technische Universität Darmstadt, Fachbereich Material und Geowissenschaften Zherebtsov, Dmitry; South Ural State University Haarmann, Frank; RWTH Aachen, Institut für Anorganische Chemie Niewa, Rainer; Universität Stuttgart, Anorganische Chemie
Keywords:	Nitride, Lithium, Li motional processes, Solid state NMR spectroscopy, Quantum mechanical calculations

ARTICLE

DOI: 10.1002/zaac.200((will be filled in by the editorial staff))

Synthesis, Crystal Structure and Li Motion of Li_8SeN_2 and Li_8TeN_2

Daniel Bräunling,[a] Oliver Pecher,[b] Dmytro M. Trots,[c] Anatoliy Senyshyn,[d] Dmitry A. Zherebtsov,[e] Frank Haarmann,[f] and Rainer Niewa*[g]

Dedicated to Prof. Dr. Rüdiger Kniep on the Occasion of his 65th birthday

Keywords: Lithium, Nitride, Chalcogenide, Crystal structure, Li motional processes, Solid state NMR spectroscopy, Quantum mechanical calculations

The compounds Li_8EN_2 with E = Se, Te were obtained in form of orange microcrystalline powders from reactions of Li_2E with Li_3N. Single crystal growth of Li_8SeN_2 additionally succeeded from excess Li. The crystal structures were refined using single crystal X-ray diffraction as well as X-ray and neutron powder diffraction data ($I4_1md$, No. 109, Z = 4, Se: a = 7.048(1) Å, c = 9.995(1) Å, Te: a = 7.217(1) Å, c = 10.284(1) Å). Both compounds crystallize as isotypes with an anionic substructure motif known from cubic Laves phases and Li distributed over four crystallographic sites in the void space of the anionic framework. Neutron powder diffraction pattern recorded in the temperature range from 3 K to 300 K and X-ray diffraction patterns using synchrotron radiation taken from 300 K to 1000 K reveal the structural stability of both compounds in the studied temperature range until decomposition. Motional processes of Li atoms in the title compounds have been revealed by temperature dependent NMR spectroscopic investigations. Those are indicated by significant changes of the ^{7}Li NMR signals. Li motion starts for Li_8SeN_2 above 150 K while already being present in Li_8TeN_2 at this temperature. Quantum mechanical calculations of NMR parameters reveal clearly different environments of the Li atoms determined by the electric field gradient which are sensitive to the anisotropy of charge distribution at the nuclear sites. With respect to an increasing coordination number according to 2 + 1, 3, 3 + 1, and 4 for Li(3), Li(4), Li(2), and Li(1), respectively, the values of the electric field gradients decrease. Different environments of Li predicted by quantum mechanical calculations are confirmed by ^{7}Li NMR frequency sweep experiments at low temperatures.

* Institut für Anorganische Chemie, Universität Stuttgart, Pfaffenwaldring 55, 70569 Stuttgart, Germany
Fax: ++49(0)711 / 685 64241
E-mail: rainer.niewa@iac.uni-stuttgart.de
[a] Department Chemie, Technische Universität München, Lichtenbergstraße 4, 85747 Garching, Germany
[b] Max-Planck-Institut für Chemische Physik fester Stoffe, Nöthnitzer Straße 40, 01187 Dresden, Germany
[c] Bayerisches Geoinstitut, Universität Bayreuth, Universitätsstraße 30, 95447 Bayreuth, Germany
[d] Fachbereich Material- und Geowissenschaften, Technische Universität Darmstadt, Petersenstraße 23, 64287 Darmstadt, Germany
[e] South Ural State University, Prospect Lenina 76, Chelyabinsk 454080, Russia
[f] Institut für Anorganische Chemie, RWTH Aachen, Landoltweg 1, 52074 Aachen, Germany
[g] Institut für Anorganische Chemie, Universität Stuttgart, Pfaffenwaldring 55, 70569 Stuttgart, Germany

Introduction

Lithium nitride halides are already well investigated, with emphasis on phase formation, crystal structures and lithium ion mobility. Early investigations originated from Sattlegger and Hahn in the 1960s [1, 2]. In the meantime the compounds have attracted some attention as fast solid lithium ion conductors [3 – 6]. More recent investigations in these systems elucidate structures and structural relationships of compounds that can be described with the general composition $Li_{3-2y}N_{1-y}X_y$ with X = Cl, Br, I [7 – 15]. In general, the crystal structures can be understood as products of acid-base reactions in which the framework structure of α-Li_3N [16] is broken down to units of lower dimensionality. In comparison to the investigations on lithium nitride halides, the data on lithium nitride chalcogenides are extremely rare [17, 18]. Here we present crystal structure analysis and thermal expansion for Li_8SeN_2 and Li_8TeN_2 in a wide range of temperatures obtained from X-ray, synchrotron radiation and neutron diffraction data. Additionally, we have used solid state NMR spectroscopy to probe motional processes of Li atoms. Furthermore the Li bonding situation is investigated by combined application of quantum mechanical calculations and NMR experiments.

Results and Discussion

Synthesis and composition determination

To derive optimal reaction temperatures for the preparation of the title compounds Li_8SeN_2 and Li_8TeN_2 we first carried out several DTA measurements (Fig. 1). The reaction of Li with appropriate amounts of Se or Te for the formation of Li_2E (E = Se, Te) in Ar atmosphere results in strongly exothermic reactions at 490 K and 691 K, respectively. The reactions proceed well above the melting point of pure Li, which can be taken from the measurements as endothermic effect at about 450 K. The onset-temperature for the formation of Li_2Se coincides with the melting point of Se (494 K), while the reaction with Te initiates some 30 K below the respective melting point of Te (723 K), corresponding to the formation of the eutectic melting

temperature $LiTe_3$–Te (696 K). In comparison, the phase diagram of Li–Se does not contain any eutectic with lower melting point than pure Se [19]. In both cases the reaction starts with a very sharp edge in the DTA-peak with no indication of a partial melting of Se or the Te containing eutectic, respectively, which should add some endothermic contribution. In a second series of experiments appropriate molar ratios of Li_3N were added to the mixtures of Li and *E*. The resulting DTA curve for *E* = Se shows an exothermic chemical reaction starting even slightly below the melting point of pure Li and smeared out over a much broader temperature range. For *E* = Te the reaction starts at a slightly higher temperature than observed for the binary case, but is similarly smeared out to higher temperatures. Since the reaction products contained significant amounts of the binary compounds next to the ternary products the higher preparation temperature of 1023 K was chosen to achieve complete reaction. The products were microcrystalline orange powders with a slightly darker color for the tellurium compound. Chemical analyses of the obtained powder samples revealed very minor impurities of oxygen and resulted in the following compositions: $Li_{7.90(6)}Se_{1.00(1)}N_{2.05(6)}O_{0.025(1)}$ (*w*(Li) = 33.60 ± 0.24 %, *w*(Se) = 48.41 ± 0.25 %, *w*(N) = 17.62 ± 0.51 %, *w*(O) = 0.25 ± 0.01 %) and $Li_{8.03(6)}Te_{1.00(1)}N_{2.18(4)}O_{0.0017(4)}$ (*w*(Li) = 24.94 ± 0.18 %, *w*(Te) = 57.07 ± 0.61 %, *w*(N) = 13.66 ± 0.25 %, *w*(O) = 0.12 ± 0.03 %). Under the identical preparation conditions, but with an excess of Li single crystals of Li_8SeN_2 were obtained.

Crystal chemistry

For crystal structure refinements in-house X-ray powder patterns were indexed with tetragonal unit cells of *a* = 7.060(2) Å, *c* = 9.9689(7) Å, *V* = 496.85(9) Å^3 (Se), *a* = 7.2127(3) Å, *c* = 10.2793(4) Å, *V* = 534.76(2) Å^3 (Te). At this point it is worthwhile to point out that those cells are metrically quite close to cubic, particularly for Li_8SeN_2, however, the reflection splitting can be clearly observed on close inspection. We note, that a similar cubic unit cell was reported for Li_7IN_2 [2]. The structure of this iodide was described in space group $F\bar{4}3m$ with a highly disordered Li-substructure [15]. For the title compounds an analysis of the extinction conditions for X-ray powder as well as single crystal data led to the tetragonal space group $I4_1/amd$ as the most likely choice. However, only the positions of the heavier anions could be determined from the X-ray diffraction data. *E* and N realize the same motif as was deduced for I and N in Li_7IN_2. With the aim to localize all Li positions we performed neutron powder diffraction at ambient and lower temperatures down to 3 K. Close inspections of the patterns revealed the presence of the reflection with Miller index (310). This reflection violates the extinction condition for the *a*-glide plane perpendicular to [001] (*hk*0: *h* = 2*n*), indicating $I4_1md$ as the correct space group choice. Apparently, the intensity contributions of Li in the neutron powder diffraction experiments produce this reflection (b_c(Li) = –1.90 fm; b_c(N) = 9.36 fm; b_c(Se) = 7.97 fm; b_c(Te) = 5.80 fm [20]) which has too low intensity to be observed in X-ray powder diffraction due to the small scattering contribution of Li. In other words, the anionic substructure is (approximately) centrosymmetric, while the Li-substructure is acentric. With this information the positional parameters of all atoms could be deduced from geometric considerations and refined against both powder diffraction patterns and single crystal X-ray diffraction data. Tabs. 1 and 2 gather crystallographic and technical data for the structure determination of Li_8SeN_2 from single crystal X-ray diffraction. Tabs. 3 and 4 present the respective data for simultaneous Rietveld refinements of X-ray and neutron powder patterns at ambient temperature for both compounds and for neutron diffraction patterns at 3 K. Fig. 2 graphically depicts exemplarily the results of the Rietveld refinements for Li_8TeN_2 based on simultaneous treatment of X-ray and neutron powder diffraction patterns taken at 300 K. Refinement data on neutron diffraction patterns for further temperatures are available as supplementary data. After those structure refinements were finished it came to our knowledge, that neutron powder diffraction at ambient temperature had earlier been carried out in the frame of a habilitation thesis [17]. The resulting structural data are nearly identical.

According to our structure refinements Li_8SeN_2 and Li_8TeN_2 are isotypes. In the following we will discuss the structure peculiarities by using the distances from simultaneous X-ray and neutron powder diffraction, since the positions of Li should be more precisely determined. For sake of simplification we use the distances in Li_8TeN_2, the corresponding distances for Li_8SeN_2 can be taken from Tab. 5. Fig. 3 utilizes anisotropic displacement parameters from the single crystal diffraction refinement to emphasize the displacement of Li atoms.

The anionic substructure of N and *E* resembles the atomic arrangement in cubic Laves phases, e.g., $MgCu_2$. N occupies the position of Cu leading to a three-dimensional framework of vertex-sharing (empty) tetrahedra (Fig. 4). These tetrahedra are significantly distorted with edge lengths in the range of 3.3175(5) Å to 3.8736(5) Å. The chalcogenide atoms are localized in the large voids of this frame within so-called Friauf polyhedra.

Li atoms fill the space within the anionic framework leading to the quite high coordination number of 9 for nitrogen (for comparison in α-Li_3N: *CN*(N) = 8 [16], for the modifications at higher pressures β-Li_3N: *CN*(N) = 11, γ-Li_3N: *CN*(N) = 6 + 8 [21]) in a distorted capped quadratic antiprism. The interatomic distances are with *d*(Li–N) = 2.090(6) Å – 2.225(6) Å slightly longer than in α-Li_3N, which can be easily rationalized from the different coordination numbers for N. Under consideration of Li–Te distances *d*(Li–Te) < 3 Å for the first coordination sphere (Li_2Te: *d*(Li–Te) = 2.82 Å [22]) Te is coordinated by 9 Li in a capped tetragonal cuboid (Fig. 5). However, the surrounding of the four crystallographic positions of Li are largely different (Fig. 3): considering the same maximum distances *d*(Li–Te) < 3 Å Li(1) is tetrahedrally coordinated by 2 N and 2 Te and Li(2) is in trigonal somewhat non-planar coordination by N (angular sum 341.5°) completed by a Te at a clearly longer distance of 3.24(1) Å. The surrounding of Li(4) is trigonal planar formed by two N and one Te. Different from those environments is the Li(3) coordination by two N with a bonding angle of 154.13(3)°. This two-fold coordination is indicated by distances below 2 Å and the longer distance to Te of 3.19(1) Å. As is also indicated by quantum mechanical calculations and NMR spectroscopic investigations this arrangement leads to a clearly different bonding situation as compared to the three other Li sites (cf. NMR part).

The relation to the cubic Laves phase $MgCu_2$ can be most comfortably be derived in terms of a group-subgroup scheme after Bärnighausen [23] as is depicted in Fig. 6. Starting from the space group type $Fd\bar{3}m$ of the Laves phase $MgCu_2$ the tetragonal space group $I4_1/amd$ results from a *translationsgleiche* symmetry reduction with index 3 with $a' = (a - b)/2$, $b' = (a + b)/2$, $c' = c$. A second *translationsgleiche* reduction with index 2 leads to the non-centrosymmetric space group $I4_1md$ and the respective positions of the anions in Li_8ENe_2.

The crystal structure of the title compounds resemble that of the structure family of Argyrodites (mineral Ag_8GeS_6 [24]). In the cubic high-temperature phases (space group $F\bar{4}3m$) of Argyrodites the chalcogenide realizes the motif a three-dimensional tetrahedral network of edge-sharing tetrahedra in the arrangement of Cu in the cubic Laves phase $MgCu_2$. However, these tetrahedra are partly filled by Ge leading to a stacking of tetrahedra GeS_4 and further S. Argyrodites are extremely flexible in their compositions. They may be described with the general formula $A_{(12-n)}B^{n+}E^{2-}{}_{(6-y)}X^-_y$ with e.g. A = Li, Cu, Ag; B = P, As, Si, Ge; E = S, Se; X = Cl, Br, I and generally are known as Cu-, Ag- and Li-ionic conductors [25, 26].

A number of cubic Laves phases are able to intercalate significant amounts of hydrogen under preservation of the general structural motif of the metal atoms although undergoing crystallographic symmetry reductions [27]. In the context of the title compounds it is particularly interesting to compare with the hydrogen-rich compounds $LaMg_2D_7$, $CeMg_2D_7$ [28] and $SmMg_2D_7$ [29]. Upon hydride formation the cubic Laves phases distort to tetragonal metric with space group $P4_12_12$. In the resulting crystal structures the deuterium occupies positions in trigonal planar and tetrahedral coordination by either exclusively Mg or rare-earth metal and Mg. However, one crystallographic site is situated in the tetrahedra formed by Mg. This position is unoccupied in Li_8ENe_2 (while it is partly occupied by Ge in the aforementioned Argyrodites). Nevertheless, the rare-earth metal in the deuterides is higher coordinated by D (twelve-fold) than E by Li in the title compounds (nine-fold). On the other hand Mg is seven-fold and N nine-fold coordinated, respectively. This example underlines the structural stability of the Laves phase arrangement if a reasonable radii ratio is provided together with an extremely high structural variety for intercalation of small atoms.

Temperature dependent diffraction experiments

Since the displacement parameters of particularly Li at room temperature are comparably large we have studied the crystal structures of the title compounds additionally by neutron diffraction at 3, 50, 100, 150, 200, 250 K to derive a reliable structure model. No indication for a structural transition was observed in these measurements. This finding agrees with the fact that DSC measurements in the temperature range of 175 K – 670 K did not show any significant signal possibly related to a phase transition. On cooling the *c*/*a* ratio monotonically decreases, however, the ideal value of $\sqrt{2}$ for a cubic metric is not reached even at 3 K (Figs. 7 and 8). Fig. 9 shows the temperature dependence of the isotrope displacement parameters as exclusively derived from these neutron diffraction experiments. Besides some scatter, all displacement parameters shrink with decreasing temperature. However, extrapolation of the values for N and E to zero K results in small but finite values. The extrapolated displacement parameters for the different sites occupied by Li give quite large values indicating a significant static contribution additional to the vibration dominating at higher temperatures.

High-resolution powder diffraction studies at elevated temperatures up to 1000 K were carried out applying synchrotron radiation. Again the data indicate no structural transition in the studied temperature range in agreement with DSC measurements. At ambient temperatures the curves nearly coincide with those from neutron powder diffraction with only a small offset. With increasing temperature the unit cell parameters monotonically increase (Figs. 7 and 8). However, above 500 K the *c*/*a* ratio exhibits a kink to a different slope followed by a maximum at 700 K and a decreasing ratio at higher temperatures. At such high temperatures the title compounds slowly decompose under formation of Li_2E, the unit cell volume of Li_8ENe_2 determined at room temperature after the heating circle is slightly smaller than the initial volume indicating a slight change of composition. Simultaneously, the colors of the samples slightly darken. Li_8ENe_2 expands quite normally under heating up to ~800 K and expansion increases in the range where the second phase appears. Relative expansion parameters along the *a*- and *c*-axes indicate a nearly isotropic behavior in the studied temperature range until onset of decomposition.

NMR spectroscopy and quantum mechanical calculations

To study the chemical bonding of the different Li atoms in Li_8SeNe_2 and Li_8TeNe_2 NMR spectroscopy in combination with quantum mechanical calculations was applied. This approach was successfully used in the past for various classes of compounds [30 – 32]. Since the title compounds are electrically non-conducting, chemical shielding (δ) and electric field gradient (EFG) can be calculated with quantum mechanical methods [33 – 35]. This allows an estimation of the expected NMR signals and provides information about the bonding situation of the atoms.

The results of the quantum mechanical calculations of NMR parameters for the structure models obtained via neutron powder diffraction at 3 K and the geometrically optimized structures of Li_8SeNe_2 and Li_8TeNe_2 are very similar for both compounds (Tab. 6). The bonding situations of the Li atoms at the four different sites apparently differ since their EFGs vary considerably. A visualization of the EFGs as ellipsoids with respect to their environment is depicted exemplarily for Li_8TeNe_2 in Fig. 10. To emphasize the orientation of the tensors which for powder samples can only be obtained by quantum mechanical calculations the directions of the three principal axes V_{ii} are indicated. No significant differences of the orientations were obtained for Li_8SeNe_2 indicating a high similarity of the bonding situation of the Li atoms in both compounds. The sizes of the ellipsoids corresponding to the anisotropy of the charge distribution at the nuclear sites clearly decrease with increasing coordination number according to $CN = 2 + 1$, $3 + 1$, and 4 for Li(3), Li(4), Li(2), and Li(1), respectively. The large EFG of Li(3) indicates an outstanding anisotropy of the charge distribution compared to the other Li atoms. For comparison the EFGs in α-Li_3N determined by NMR experiments are 0.58 MHz and 0.28 MHz for the two-fold

and the three-fold coordinated Li atoms, respectively [36]. Quantum mechanical calculations are in good agreement with these results. The origin of the EFGs was attributed to a polarization of the charge distribution of the Li atoms [30]. This polarization induced by chemical bonding can also be expected to be the largest for Li(3) in Li_8SeN_2 and Li_8TeN_2 since the Li–N distances of 1.955(8) Å and 1.990(3) Å, respectively, are significantly shorter than for the other Li atoms (Tab. 5). This corresponds to the situation in α-Li_3N with 1.939 Å and 2.130 Å for the two-fold and three-fold coordinated Li atoms, respectively [16]. Considering the different values of the EFGs of the title compounds the Li environments might be distinguishable by NMR experiments.

The non-referenced calculated isotropic chemical shifts (δ_{iso}) are quite similar for all Li atoms, thus it can not be expected to resolve separated NMR signals experimentally. With respect to the anisotropy of chemical shielding (δ_{aniso}) Li(3) also differs from the other Li indicating an exceptional bonding situation of Li(3) (Tab. 6).

The static and magic angle spinning (MAS) ^{7}Li NMR signals of Li_8SeN_2 and Li_8TeN_2 recorded at ambient temperature are depicted in Fig. 11. The full spectral width of the signals indicates the presence of quadrupole coupling being due to interactions of the EFG at the nuclear sites with the nuclear quadrupole moments. This can also be seen by the number of rotational side bands of the MAS NMR signals. The main transition in the centre of the signal is almost symmetric and covers a comparably small frequency range being in agreement with simulations of the NMR signals based on the quantum mechanical calculations. The individual signal contributions can not be resolved by application of MAS, but the average isotropic chemical shift can be determined (see Tab. 6 and inset of Fig. 11).

To investigate motional processes of the Li atoms temperature dependent NMR experiments were performed. The full width at half maximum (FWHM) of the NMR signals for both compounds differs significantly at ambient temperature (Fig. 11 inset). Assuming dipole-dipole coupling to be the dominant mechanism of the NMR signal line broadening this already indicates motional processes of the Li atoms which average the coupling. The temperature dependence of the FWHM and the corresponding ^{7}Li NMR signals show a dramatic change of the NMR signal line shape (Fig. 12). At low temperatures the main transition signal is broadened and the satellite transitions are clearly visible, resulting in an elaborated line shape of the NMR signals. At high temperatures only a narrow NMR signal remains for both compounds. The change of the NMR signal line shape indicates an averaging of the quadrupole coupling in addition. A continuous decrease of the FWHM of the main transition NMR signal with increasing temperature is observed for Li_8SeN_2 and Li_8TeN_2 (Fig. 12 insets). In contrast a dramatic reduction of the FWHM resulting from a spontaneous onset of Li diffusion accompanied by a phase transition is reported e.g. for the Argyrodite Li_6PS_5I [37, 38]. The continuous change of the FWHM for the title compounds evidences the absence of a phase transition of the title compounds being in agreement with the diffraction experiments.

The decrease of the signal width with temperature differs for Li_8SeN_2 and Li_8TeN_2 (Fig. 12 insets). While for Li_8SeN_2 a constant signal width seems to be reached below 150 K it is not yet clear for which temperature a constant FWHM of the Li_8TeN_2 NMR signals is reached since the values decrease with increasing temperature in the investigated temperature range. Additional NMR measurements of the FWHM at lower temperatures are required for this purpose. Above 350 K and 450 K a constant signal width is observed for Li_8SeN_2 and Li_8TeN_2, respectively. This indicates differences of the motional processes of the Li atoms for both compounds.

In order to resolve the different ^{7}Li NMR signal contributions and to ensure that the motional processes of the Li atoms are frozen, frequency sweep NMR experiments were performed at 15 K (Fig. 13). Remarkably different NMR line shapes for both compounds are observed at this temperature. While the NMR signal of Li_8TeN_2 is well elaborated showing clearly the features of the individual signal contributions, the signal of Li_8SeN_2 is smeared out and characteristic features of the signal contributions are only weekly indicated. This difference points at a high level of residual disorder in Li_8SeN_2 and is confirmed by detailed line shape analysis of the NMR signals. Using the results of the quadrupole coupling parameters obtained by the quantum mechanical calculations as a starting model the experimental values were quantified by least-squares fits of the NMR signals (Tab. 6). Both NMR experiments and quantum mechanical calculations are in good agreement confirming experimentally the anisotropy of the charge distribution in the vicinity of the nuclear sites of the Li atoms determined by quantum mechanical methods.

Concluding remarks

The title compounds show Li-motional processes according to solid state NMR spectroscopy. An anomalous thermal expansion in non-ion conducting phases, which precedes a transition to an ion conducting phase, seems to be characteristic for some solid ion conductors (see [39] and references therein), in particular when they undergo an abrupt transition into the ion conducting state. The compounds Li_8EN_2 (E = Se, Te) do not suffer any clearly recognizable transition in the full temperature range from 3 K to close to 800 K according to diffraction data. The observation of Li motion by NMR spectroscopy without a sharp structural transformation to an ion conducting phase could imply that Li_8TeN_2 and Li_8SeN_2 are type II or type III ion conductors according to classification by Keen [40].

The anisotropy of the charge distribution of the Li atoms differs considerably for the four crystallographic sites in Li_8EN_2 with E = Se and Te, respectively. A clear correlation of the anisotropy of the charge distribution and the coordination number of the Li atoms is recognized. Good agreement of NMR experiments and quantum mechanical calculations of NMR parameters is obtained.

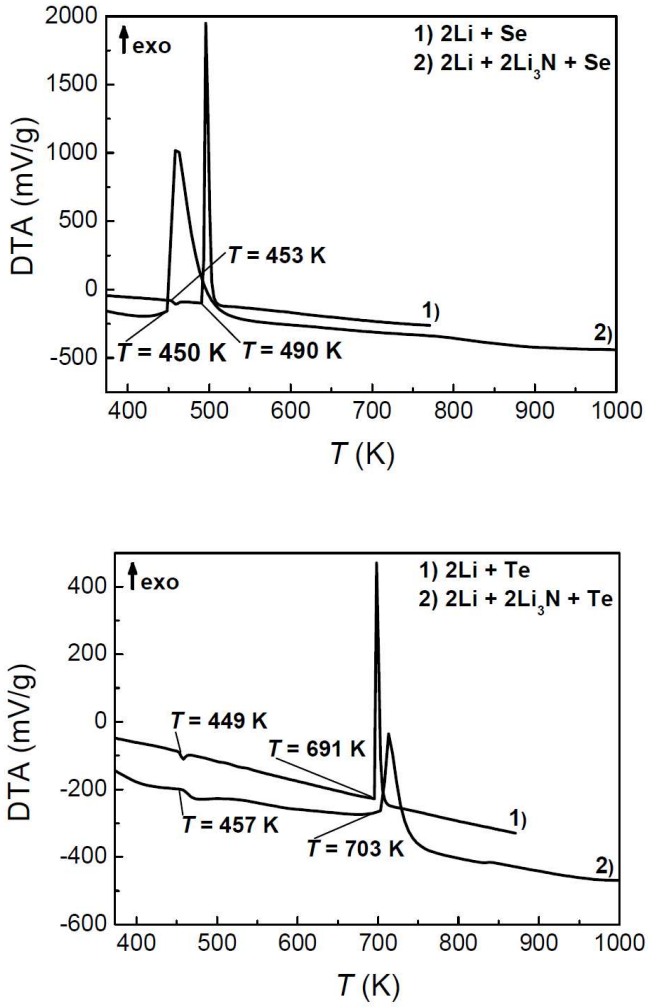

Figure 1. DTA diagrams of reactions of (1) Li with *E* and (2) Li, *E* with Li_3N (top: *E* = Se, bottom: *E* = Te).

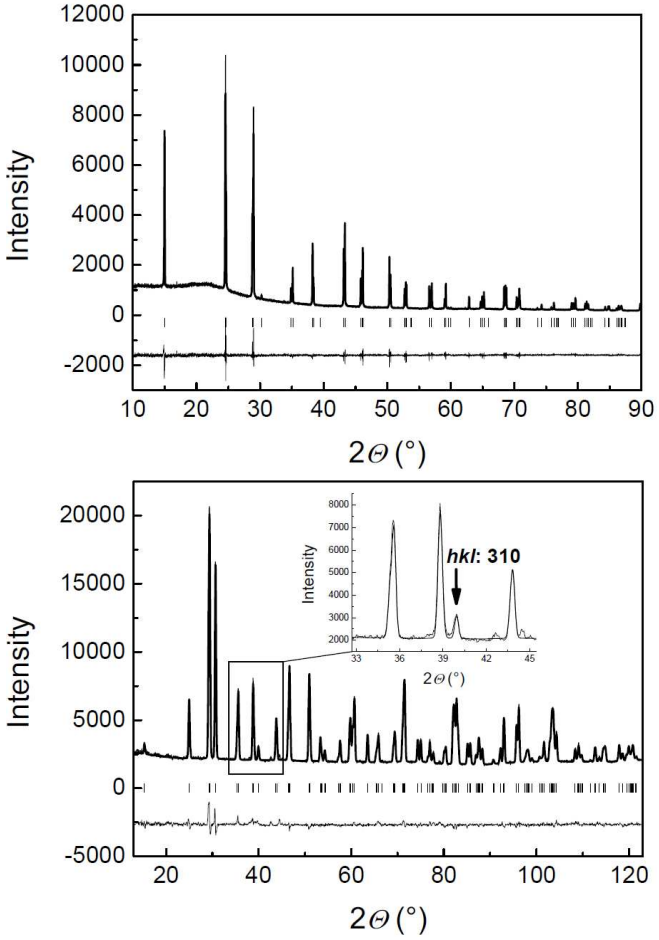

Figure 2. Li_8TeN_2: X-ray ($CuK\alpha_1$ radiation, top) and neutron (λ = 1.5482 Å, bottom) powder diffraction diagrams. The measured data are shown as points, the continuous line represents the calculated profile and the lower line shows the difference between the calculated and observed intensities. Marks below the data indicate positions of calculated Bragg reflections. The inset enlarges the reflection (310) calling for the space group choice $I4_1md$ rather than $I4_1/amd$ (low intensity reflections at 2theta of about 42.8° and 44.8° are due to a minor unknown impurity).

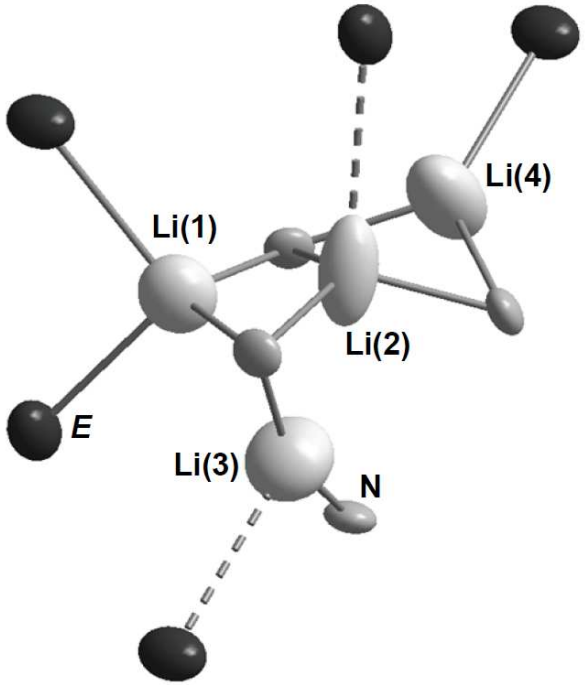

Figure 3. Li_8SeN_2: Coordination of Li (large grey ellipsoids) by N (smaller grey ellipsoids) and Se (dark ellipsoids). Interatomic distances > 3 Å are indicated by dashed lines. Anisotropic displacement ellipsoids are taken from the single crystal X-ray data and depicted with 99 % probability.

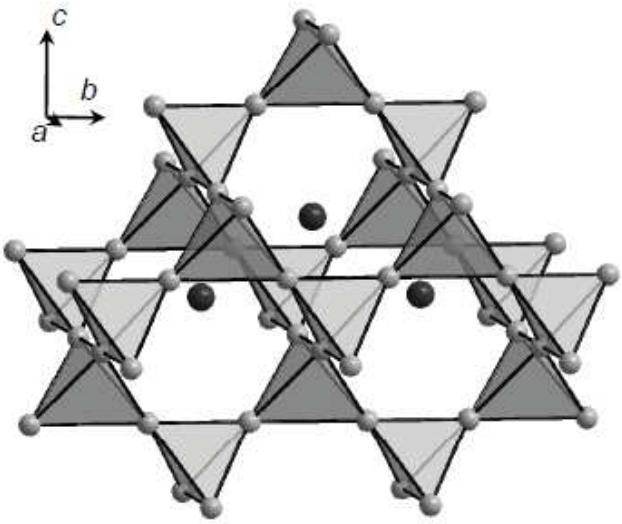

Figure 4. Li_8EN_2: Chalcogenide ions E = Se, Te (dark spheres) embedded in a framework of vertex-sharing (empty) tetrahedra of N (light grey spheres) with the structural motif of a cubic Laves phase.

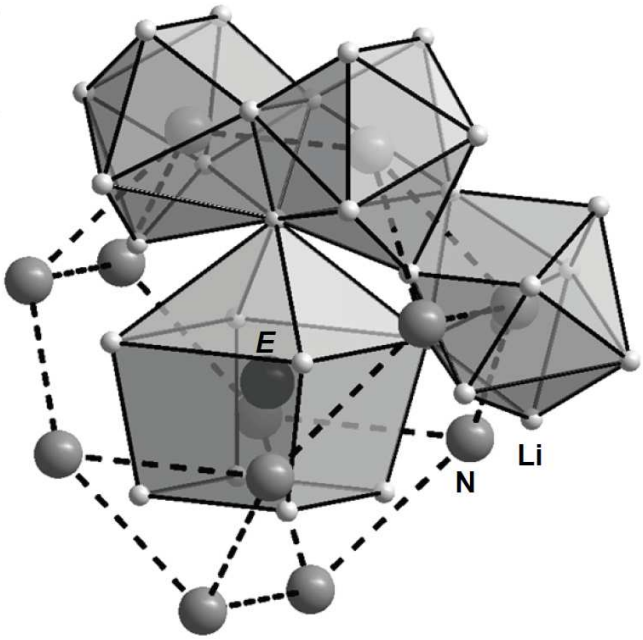

Figure 5. Li_8EN_2: Capped cuboid as first coordination environment of E = Se, Te (dark spheres) by Li (small light grey spheres). The second coordination (Friauf polyhedron) formed by N (larger grey spheres) is indicated by dashed lines. Exemplarily, the coordination of three N by Li in form of distorted capped square anti-prisms given.

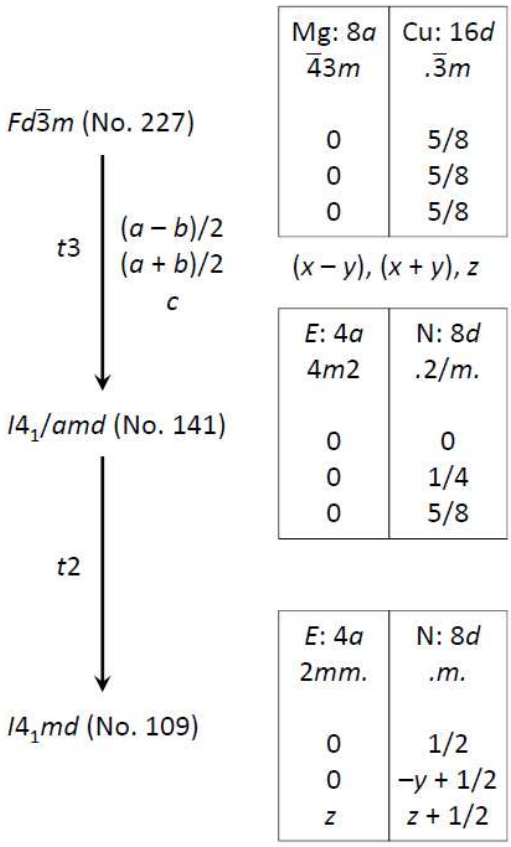

Figure 6. Li_8EN_2: Group-subgroup scheme [23] for the anionic substructure derived from the cubic Laves phase $MgCu_2$. The left part represents the symmetry reduction (*translationsgleiche* (*t*) and index) and unit cell transformation. The relationship between the atomic coordinates is shown on the right.

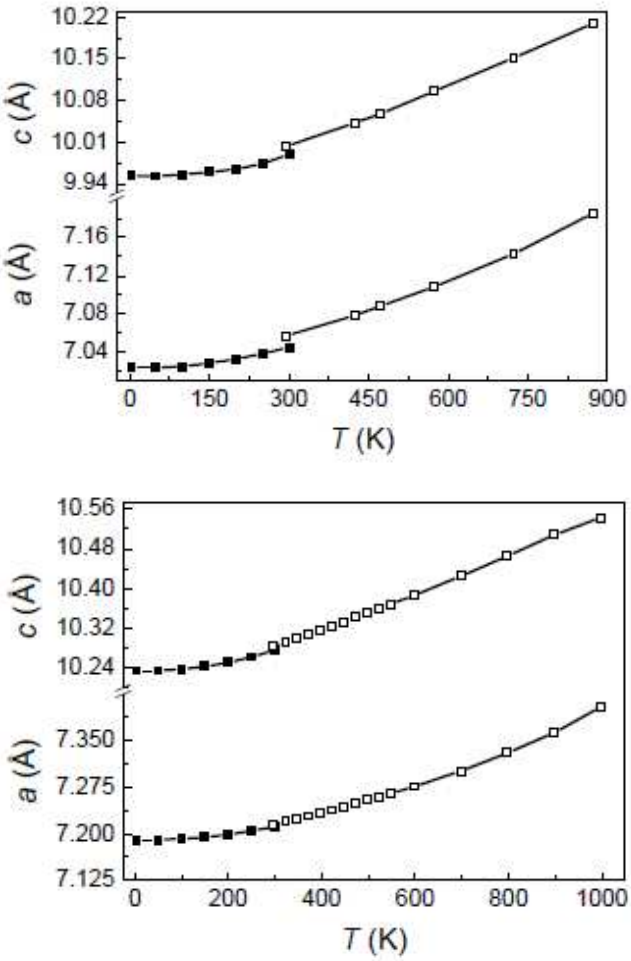

Figure 7. Li_8ENe_2: Temperature dependence of the unit cell parameters *a* and c from neutron powder diffraction (full symbols) and from high resolution X-ray powder diffraction using synchrotron radiation (open symbols) for top: *E* = Se, and bottom: *E* = Te.

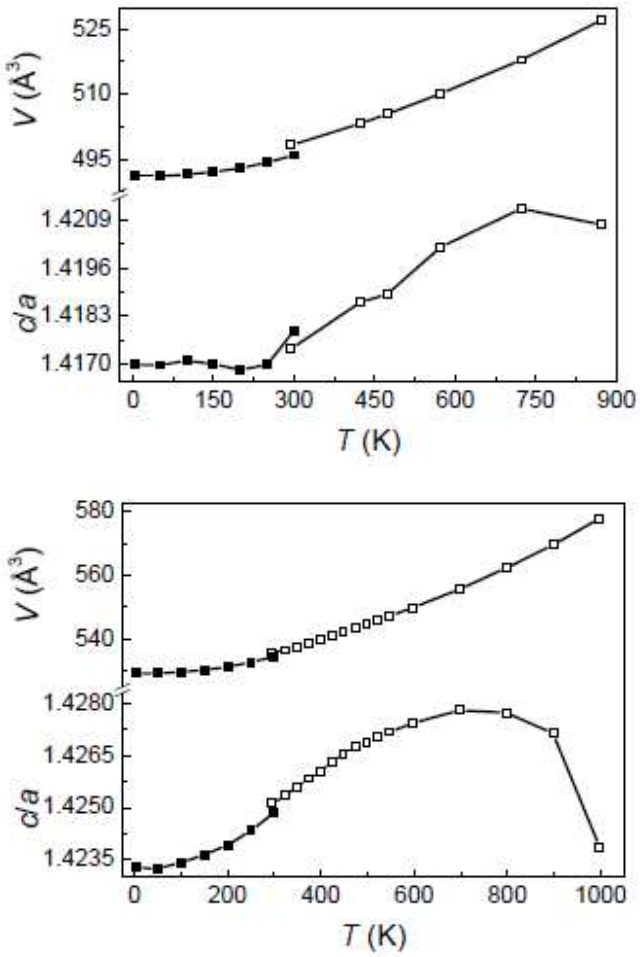

Figure 8. Li_8ENe_2: Temperature dependence of the unit cell volume *V* and the ration *c*/*a* from neutron powder diffraction (full symbols) and from high resolution X-ray powder diffraction using synchrotron radiation (open symbols) for top: *E* = Se, and bottom: *E* = Te.

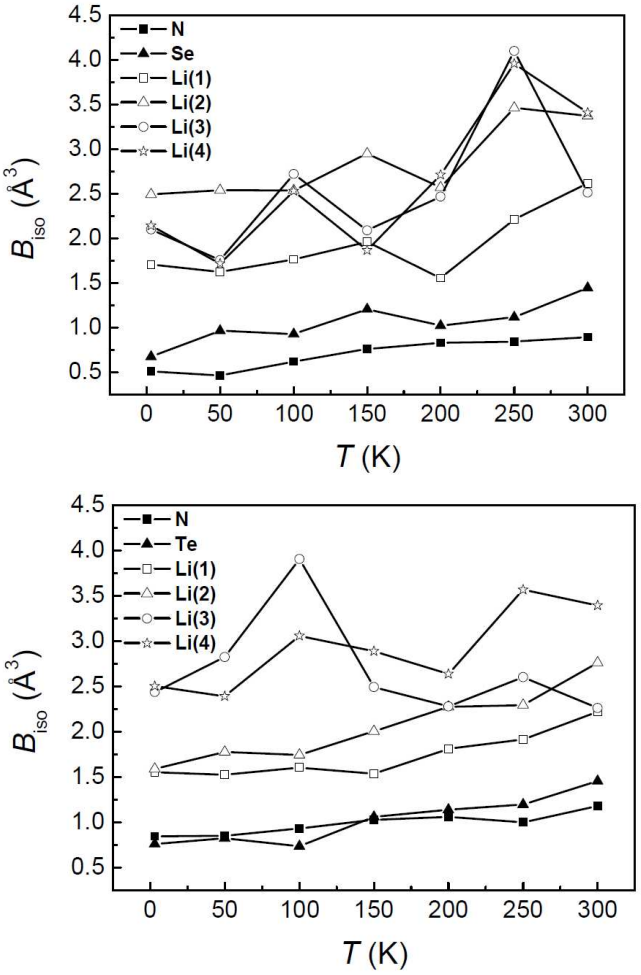

Figure. 9. Li_8ENe_2: Temperature dependence of the isotropic displacement parameters from neutron powder diffraction (top: E = Se, and bottom: E = Te).

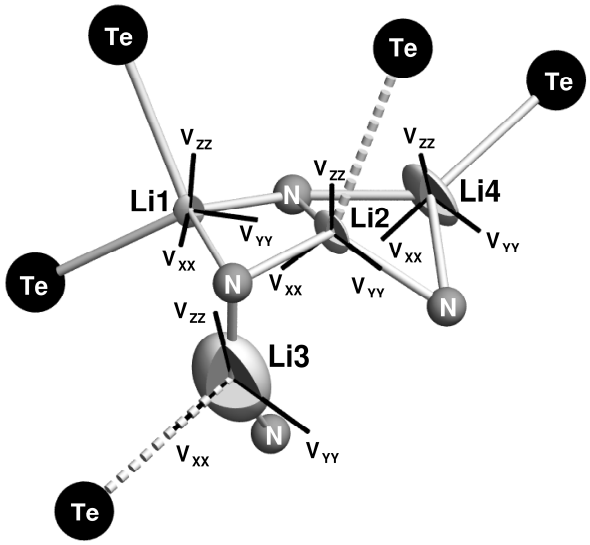

Figure 10. Visualization of the EFGs by ellipsoids obtained from quantum mechanical calculations for the geometrically optimized structure of Li_8TeN_2. The spatial orientations of the principal axes V_{ii} are indicated.

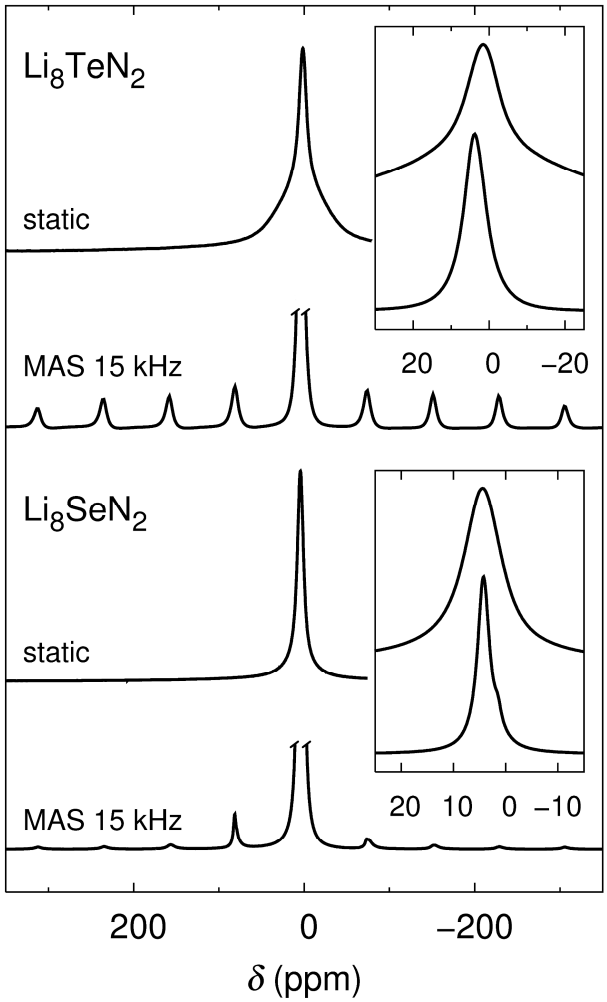

Figure 11. Static and MAS ^{7}Li NMR signals for Li_8SeN_2 and Li_8TeN_2.

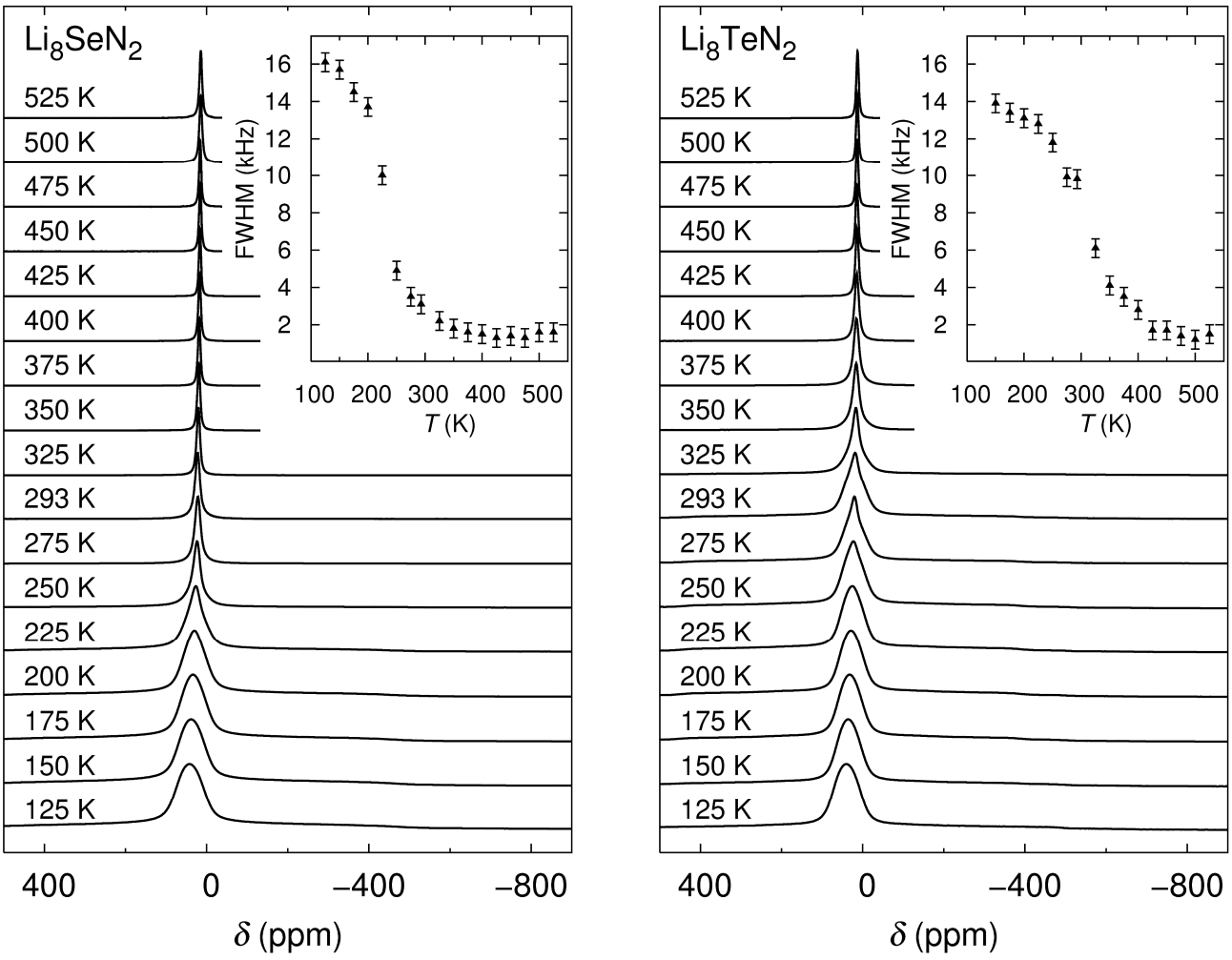

Figure 12. Temperature dependent ^{7}Li NMR measurements of Li_8SeN_2 (left) and Li_8TeN_2 (right) with an analysis of the full width at half maximum (FWHM) as a function of temperature (inset). Error bars of ± 0.5 kHz for the FWHM are indicated.

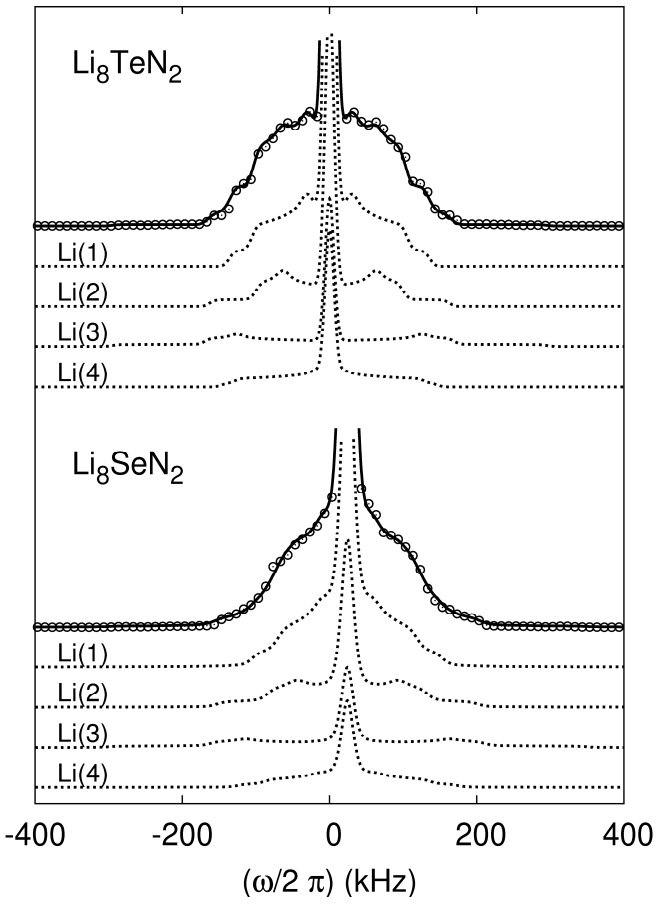

Figure 13. ^{7}Li frequency sweep NMR measurements at T = 15 K for Li_8SeN_2 (bottom) and Li_8TeN_2 (top). Data points of the various experiments are indicated by open circles. The full line represents the result of the least-squares fit and the dashed lines the individual signal contributions.

Table 1. Li_8SeN_2: Crystal structure data from single crystal X-ray diffraction.

Formula	Li_8SeN_2
Cryst. size, mm^3	$0.05 \times 0.05 \times 0.03$
Crystal system	Tetragonal
Space group	$I4_1md$ (No. 109)
a, Å	7.060(2)
c, Å	9.9689(7)
V, $Å^3$	496.85(9)
Z	4
D_{calcd}, g cm^{-3}	2.172
$\mu(MoK_\alpha)$, mm^{-1}	7.38
T, K	298
hkl range	±11, ±11, ±16
$2\theta_{max}$, deg	70.1
Refl. measured	3949
Refl. unique	606
R_{int}	0.076
Param. refined	34
BASF	0.02(4)
$R(F)/wR(F^2)$	0.043/0.070
GooF (F^2)	1.19
$\Delta\rho_{fin}$, e $Å^{-3}$	1.64

Table 2. Li_8SeN_2: Positional parameters and displacement parameters U_{ij} and U_{eq} (in $Å^2$) from single crystal X-ray diffraction.

Atom	Site	x	y	z	U_{11}	U_{22}	U_{33}	U_{12}	U_{13}	U_{23}	U_{eq}
Se	4*a*	0	0	0.89813(9)	0.0093(5)	0.0193(5)	0.0109(2)	0	0	0	0.0132(1)
N	8*b*	½	0.2671(6)	0.0003(3)	0.011(1)	0.007(2)	0.006(2)	0	0	0.003(2)	0.0079(7)
Li(1)	16*c*	0.7644(9)	0.188(1)	0.0773(6)	0.021(3)	0.024(3)	0.018(3)	0.002(2)	–0.002(2)	0.003(2)	0.021(1)
Li(2)	8*b*	½	0.151(2)	0.191(1)	0.013(4)	0.032(5)	0.029(4)	0	0	0.018(4)	0.025(2)
Li(3)	4*a*	½	0	0.962(2)	0.029(8)	0.019(7)	0.030(8)	0	0	0	0.026(3)
Li(4)	4*a*	½	0	0.383(2)	0.022(6)	0.05(1)	0.016(7)	0	0	0	0.029(4)

Table 3. Selected data of Rietveld refinements: simultaneous X-ray and neutron diffraction refinements at 300 K and single neutron diffraction refinements at 3 K. Number of refined structural parameters: 17. Radiation: Cu$K\alpha_1$ or λ = 1.5482 Å, respectively.

Composition	Li_8SeN_2			Li_8TeN_2		
	X-ray	neutron	neutron	X-ray	neutron	neutron
	300 K		3 K	300 K		3 K
Unit cell parameter a, Å	7.048(1)		7.024(1)	7.217(1)		7.190(1)
Unit cell parameter c, Å	9.995(1)		9.953(1)	10.284(1)		10.234(1)
2θ-range, deg	10.1 – 90.0	22.3 – 125.0	22.3 – 125.0	10.1 – 90.0	12.3 – 124.0	12.3 – 124.0
Step size, deg	0.01	0.05	0.05	0.01	0.05	0.05
χ^2	11.4		6.99	3.17		3.53
$R_{profile}$ R_{Bragg}	0.107, 0.098	0.041, 0.058	0.023, 0.038	0.064, 0.061	0.036, 0.057	0.022, 0.035

Table 4. Li_8ENe_2: Positional parameters and isotropic displacement parameters B_{eq} (in Å^2). First line from simultaneous X-ray and neutron powder diffraction at 300 K, second line in bold from neutron powder diffraction at 3 K.

Atom	Site	*x*	*y*	*z*	B_{eq}
Se	4*a*	0	0	0.8983(5)	1.22(7)
				0.8981(3)	**0.67(4)**
N	8*b*	½	0.2678(3)	0	0.77(4)
			0.2681(2)		**0.51(2)**
Li(1)	16*c*	0.772(1)	0.183(2)	0.077(1)	2.3(1)
		0.775(1)	**0.182(1)**	**0.077(1)**	**1.7(1)**
Li(2)	8*b*	½	0.152(2)	0.199(2)	3.3(3)
			0.154(1)	**0.199(1)**	**2.5(2)**
Li(3)	4*a*	½	0	0.949(3)	2.9(5)
				0.950(2)	**2.1(3)**
Li(4)	4*a*	½	0	0.398(3)	3.2(6)
				0.398(2)	**2.1(3)**
Te	4a	0	0	0.8969(3)	1.20(2)
				0.8962(1)	**0.76(2)**
N	8b	½	0.2686(2)	0	1.20(2)
			0.2693(1)		**0.84(1)**
Li(1)	16c	0.7541(8)	0.1871(9)	0.0787(6)	1.7(1)
		0.7583(4)	**0.1866(4)**	**0.0778(3)**	**1.55(5)**
Li(2)	8b	½	0.157(1)	0.193(1)	2.5(1)
			0.1549(6)	**0.1939(4)**	**1.58(7)**
Li(3)	4a	½	0	0.957(1)	2.9(3)
				0.9560(7)	**2.4(1)**
Li(4)	4a	½	0	0.373(1)	3.7(4)
				0.3805(7)	**2.5(1)**

Table 5. Li_8ENe_2: Selected interatomic distances (in Å) from simultaneous X-ray and neutron powder diffraction at 300 K. First line: *E* = Se, second line in bold: *E* =Te.

N–Li(1)	2.15(1)	2 ×	*E*–N	≥ 3.990(4)	
	2.090(6)			**≥ 4.231(1)**	
N–Li(1)	2.17(1)	2 ×			
	2.25(6)		*E*–Li(1)	2.73(1)	4 ×
N–Li(2)	2.02(1)	2 ×		**2.910(6)**	
	2.098(8)		*E*–Li(1)	2.84(1)	4 ×
N–Li(2)	2.15(2)	1 ×		**2.956(6)**	
	2.15(1)		*E*–Li(4)	2.50(4)	1 ×
N–Li(3)	1.955(8)	1 ×		**2.81(1)**	
	1.990(3)				
N–Li(4)	2.20(2)	1 ×			
	2.10(1)				

Table 6. ^{7}Li NMR parameters for Li_8SeN_2 and Li_8TeN_2 obtained by quantum mechanical calculations and least-square fits of the low temperature frequency sweep NMR signals (experiment). The isotropic shift δ_{iso}, anisotropy δ_{aniso} and asymmetry parameter η_δ of the chemical shielding as well as the quadrupolar coupling constant C_Q and the asymmetry parameter of the quadrupolar coupling η_Q for the Li sites are given. The sign of the quadrupolar coupling constant can not be determined by NMR experiments. The average referenced isotropic shift of the Li atoms is determined by the maxima of the MAS signals recorded at ambient temperature using a rotation frequency of 15 kHz. The calculated isotropic shifts are not referenced. Only the differences of the individual calculated values are of interest for that reason.

	Li_8SeN_2					Li_8TeN_2				
	δ_{iso} / ppm	δ_{aniso} / ppm	η_δ	C_Q / MHz	η_Q	δ_{iso} / ppm	δ_{aniso} / ppm	η_δ	C_Q / MHz	η_Q
Based on structure model obtained by neutron diffraction experiments at T = 3 K										
Li(1)	-84.73	-3.96	0.44	0.24	0.92	-85.16	-4.61	0.39	0.30	0.54
Li(2)	-83.40	3.78	0.17	-0.36	0.12	-83.67	3.97	0.27	-0.31	0.12
Li(3)	-82.55	-17.60	0.06	0.68	0.26	-83.93	-15.81	0.05	0.65	0.24
Li(4)	-85.16	5.15	0.52	-0.31	0.13	-85.29	5.40	0.24	-0.33	0.67
Based on geometrical optimized structure model										
Li(1)	-84.85	-4.54	0.29	0.27	0.67	-85.14	-4.95	0.35	0.32	0.46
Li(2)	-83.09	3.82	0.61	-0.37	0.20	-83.58	4.02	0.47	-0.31	0.23
Li(3)	-83.06	-18.30	0.03	0.73	0.15	-83.96	-15.99	0.03	0.66	0.22
Li(4)	-85.04	5.37	0.40	-0.34	0.56	-85.33	5.51	0.48	-0.34	0.77
Experiment										
Li(1)	4.3	-	-	0.26(2)	0.5(1)	4.0	-	-	0.27(2)	0.6(1)
Li(2)				0.35(2)	0.2(1)				0.33(2)	0.2(1)
Li(3)				0.65(2)	0.2(1)				0.59(2)	0.2(1)
Li(4)				0.30(2)	0.5(1)				0.29(2)	0.7(1)

Experimental Section

Preparation

All manipulations were carried out under dry argon in a glovebox ($p(O_2,H_2O) < 0.1$ ppm). Li_3N was prepared from elemental lithium (rods, Alfa, 99.9%) and nitrogen (Messer-Griesheim, 99.999%, additionally purified by passing over molsieve, Roth 3 Å, and BTS catalyst, Merck) of ambient pressure at 670 K. The lithium chalcogenides Li_2E (E = Se, Te) were obtained from the elements in sealed tantalum ampoules at 575 K and 775 K, respectively. For synthesis of Li_8SeN_2 and Li_8TeN_2 appropriate molar ratios of Li_3N und Li_2E were reacted at 1023 K in sealed tantalum ampoules. The products were microcrystalline orange powders with a slightly darker color for the tellurium compound. Both ternary nitrides are sensitive against moist air.
In synthesis experiments with excess Li small single crystals of Li_8SeN_2 were obtained using the above mentioned conditions.

Thermal analysis

Difference scanning calorimetry was performed on a DSC 204 Phoenix (Netzsch) in Ar-filled sealed aluminum crucibles. DTA/TG measurements (STA 409, Netzsch, Nb crucibles, thermocouple type S) were performed under nitrogen and argon to analyze the formation of the ternary compounds, to find the optimum reaction conditions, and to examine the decomposition behaviour. Temperature calibration was carried out with five melting points of pure metals.

X-ray diffraction

In-house X-ray powder diffraction pattern were taken in transmission (STADIP, STOE) with Cu$K\alpha_1$ radiation.
X-ray diffraction on a single crystal Li_8SeN_2 (sealed in a glass capillary) was performed on a MSC-Rigaku R-Axis Rapid diffractometer applying Mo$K\alpha$-radiation. An absorption correction based on symmetry-equivalent reflections was applied [41].
In situ crystal structure investigations between room temperature and 1098 K were carried out with high-resolution powder diffraction applying synchrotron radiation (beamline B2, HASYLAB at DESY). The diffraction experiments were performed in Debye-Scherrer capillary geometry with the samples sealed in quartz capillaries using an on-site readable image plate detector OBI [42]. The wavelength of 0.65131 Å was calibrated using the reflection positions of LaB_6 (NIST SRM 660a) reference material. The typical full-width at half-maximum (FWHM) of reflections obtained in this geometry was 0.06 – 0.08°. A STOE furnace was used for *in situ* HT diffraction experiments. For Li_8TeN_2 patterns were taken from room temperature to 548 K in steps of 25 K, and from 598 K to 1098 K in steps of 100K. All patterns were recorded for a duration of 9 min. Due to apparent chemical reactions of Li_8SeN_2 the measurements were restricted to a maximum of 900 K with recording times of 15 min per pattern.

Neutron powder diffraction

The samples were placed in argon-filled cylindrical vanadium containers (diameter 8 mm; length 51 mm; wall thickness 0.15 mm) and sealed with indium gaskets. Patterns were collected at 3, 50, 100, 150, 200, 250 and 300 K at the SPODI diffractometer of FRM II with the wavelength of 1.5482 Å.

Structure refinements

For all Rietveld refinements the program package FULLPROF [43] was used. For all refinements against powder data the fractional coordinate z of N (highest contribution to neutron diffraction due to high diffraction length) was fixed to zero. The crystal structure of Li_8SeN_2 based on data from single crystal diffraction intensity collection was refined with the program system SHELXL-97-2 [44].

Chemical analyses

Chemical analyses for N and O were carried out via hot-gas-extraction (LECO 436 DR). Li, Se and Te were quantified applying the inductively coupled plasma-optical emission spectrometry (ICP-OES, Varian, VISTA RL) method.

NMR spectroscopy and quantum mechanical calculations

^{7}Li NMR spectroscopic investigations were performed by using a Bruker AVANCE spectrometer with a magnetic field of B_0 = 11.74 T. The corresponding resonance frequency of the ^{7}Li isotope is 194.373 MHz. The NMR signals are referenced to a saturated solution of LiCl in D_2O.
Magic angle spinning (MAS) NMR experiments were carried out for different rotation frequencies at ambient temperature on powder samples of Li_8SeN_2 and Li_8TeN_2 filled into ZrO_2 rotors (4.0 mm diameter) using a Bruker double resonance MAS probe. Full recovery of the magnetization at ambient temperature was achieved within 1.0 s. Single pulse experiments with hard pulses of 3.5 µs duration were applied for the Se compound. An echo pulse sequence with pulses of equal duration of 2.5 µs was used for Li_8TeN_2. The interpulse delay was synchronized with the rotation frequency.
Wide line variable-temperature ^{7}Li NMR signals were recorded for randomly oriented crystallites of Li_8SeN_2 and Li_8TeN_2 enclosed in a sealed glass ampoule over a temperature range of 125 K to 525 K. Depending on the spectral width at different temperatures either single pulse experiments with hard pulses of 3.0 µs duration or an echo sequence with pulses of equal duration of 1.5 µs were applied. The interpulse distance of the echo sequence was optimized to 100 µs to avoid distortions of the NMR signal line shape.
Frequency sweep ^{7}Li NMR experiments at 15 K were performed on the powder samples of Li_8SeN_2 and Li_8TeN_2 mounted on a low-Q probe with automatic tuning and matching built by NMR-Service (Erfurt, Germany). The temperature was adjusted in a helium cryostat system. A series of selective excitation experiments was applied using low-power pulses of 100 µs.
NMR signals were simulated using the SIMPSON [45] program package using $\delta_{iso} = 1/3\ (\delta_{XX} + \delta_{YY} + \delta_{ZZ})$, $\delta_{aniso} = \delta_{ZZ} - \delta_{iso}$ and $\eta_\delta = (\delta_{XX} - \delta_{YY}) / \delta_{aniso}$ for the isotropic, the anisotropic, and the asymmetry parameter of the chemical shielding, respectively. The order of the principal axes of the shielding tensor is defined by $|\delta_{ZZ} - \delta_{iso}| \geq |\delta_{XX} - \delta_{iso}| \geq |\delta_{YY} - \delta_{iso}|$ resulting in $0 \leq \eta_\delta \leq 1$. The quadrupole coupling constant is defined as $C_Q = e\,Q\,V_{ZZ} / h$ with the nuclear quadrupole moment $Q(^7\text{Li}) = -4.01$ fm^2 [46] and the main principal component of the electric field gradient V_{ZZ}. The asymmetry parameter of the quadrupole coupling is defined as $\eta_Q = (V_{XX} - V_{YY}) / V_{ZZ}$ with $|V_{ZZ}| \geq |V_{XX}| \geq |V_{YY}|$ and $0 \leq \eta_Q \leq 1$.
Quadrupole coupling and chemical shift parameters were calculated using the NMR-CASTEP [33] code, within periodic boundary conditions and the pseudopotential approximation using the GIPAW [47] and PAW [34, 48] methods. On-the-fly generated ultrasoft pseudopotentials were used for the calculations. The calculations were performed with a cut-off energy of 450 eV and with 4 × 4 × 5 k points using GGA (PBE [49]). Geometry optimizations were also performed using the code. The model of the crystal structure obtained at 3 K using neuton powder diffraction was used as basis for the geometry optimization.

Supporting Information Unit cell parameters at different temperatures are gathered in Tables S1 – S4. Further details of the single crystal structure investigation may be obtained from Fachinformationszentrum Karlsruhe, 76344 Eggenstein-Leopoldshafen, Germany (fax: +49-7247-808-666; e-mail: crysdata@fiz-karlsruhe.de, http://www.fiz-informationsdienste.de/en/DB/icsd/depot_anforderung.html) on quoting the deposition number CSD-421252.

Acknowledgments

We would like to thank Anja Völzke for performing the chemical analyses, Susann Scharsach for DSC measurements and Yurii Prots for single crystal X-ray diffraction intensity data collection.

[1] H. Sattlegger, H. Hahn, *Z. Anorg. Allg. Chem.* **1970**, *379*, 293–299.

[2] H. Sattlegger, H. Hahn, *Naturwissenschaften* **1964**, *51*, 534–535.

[3] P. Hartwig, W. Weppner, W. Wichelhaus, *Mater. Res. Bull.* **1979**, *14*, 493–498.

[4] P. Hartwig, W. Weppner, W. Wichelhaus, A. Rabenau, *Angew. Chem. Int. Ed. Engl.* **1980**, *19*, 74–75.

[5] K. Kitahama, Y. Furukawa, S. Kawai, O. Nakamura, *Solid State Ionics* **1981**, *3/4*, 335–339.

[6] Y. Jia, J. Yang, *Solid State Ionics* **1997**, *96*, 113–117.

[7] R. Marx, *Z. Naturforsch.* **1995**, *50b*, 1061–1066.

[8] R. Marx, *J. Solid State Chem.* **1997**, *128*, 241–246.

[9] R. Marx, H. M. Mayer, *Z. Naturforsch.* **1995**, *50b*, 1353–1358.

[10] R. Marx, H. M. Mayer, *J. Solid State Chem.* **1997**, *130*, 90–96.

[11] R. Marx, R. M. Ibberson, *J. Alloys Compd.* **1997**, *261*, 123–131.

[12] R. Marx, H. M. Mayer, *Z. Naturforsch.* **1996**, *51b*, 525–530.

[13] R. Marx, *J. Alloys Compd.* **1997**, *256*, 196–206.

[14] R. Marx, *Z. Anorg. Allg. Chem.* **1997**, *623*, 1912–1916.

[15] R. Marx, *Eur. J. Solid State Inorg. Chem.* **1998**, *35*, 197–209.

[16] A. Rabenau, H. Schulz, *J. Less-Common Met.* **1976**, *50*, 155–159.

[17] R. Marx, Habilitation Thesis, Freie Universität Berlin, **2002**.

[18] R. Marx, F. Lissner, T. Schleid, *Z. Anorg. Allg. Chem.* **2006**, *632*, 2151.

[19] T. B. Massalski (Ed.): *Binary Alloy Phase Diagrams*. 2nd Ed., ASM International, Materials Park, Ohio 1990.

[20] International Tables for Crystallography, Volume C, 5th Edition, Ed. T. Hahn, Kluwer Academic Publishers, 2002.

[21] H. U. Beister, S. Haag, R. Kniep, K. Strossner, K. Syassen, *Angew. Chem. Int. Ed. Engl.* **1988**, *27*, 1101–1103.

[22] E. Zintl, A. Harder, B. Dauth, *Z. Electrochem. Angew. Phys. Chem.* **1934**, *40*, 588–593.

[23] H. Bärnighausen, *MATCH, Commun. Math. Chem.* **1980**, *9*, 139–173.

[24] V. M. Goldschmidt, *Z. Kristallogr. Mineral.* **1909**, *45*, 548–554; C. Palache, H. Berman, C. Fondel, *Dana's system of Mineralogy*, 7th Ed. **1944**, 356ff.

[25] T. Nilges, A. Pfitzner, *Z. Kristallogr.* **2005**, *220*, 281–294.

[26] H.-J. Deiseroth, S.-T. Kong, H. Eckert, J. Vannahme, C. Reiner, T. Zaiß, M. Schlosser, *Angew. Chem. Int. Ed.* **2008**, *47*, 755–758.

[27] H. Kohlmann, F. Fauth, P. Fischer, A. V. Skripov, V. N. Kozhanov, K. Yvon, *J. Alloys Comp.* **2001**, *327*, L4–L9 and references given therein.

[28] F. Gingl, K. Yvon, T. Vogt, A. Hewat, *J. Alloys Comp.* **1997**, *253*, 313–317.

[29] H. Kohlmann, F. Werner, K. Yvon, G. Hilscher, M. Reissner, G. J. Cuello, *Chem. Eur. J.* **2007**, *13*, 4178–4186.

[30] P. Blaha, K. Schwarz, P. Herzig, *Phys. Rev. Lett.* **1985**, *54(11)*, 1192–1195.

[31] F. Haarmann, K. Koch, D. Grüner, W. Schnelle, O. Pecher, R. Cardoso-Gil, H. Borrmann, H. Rosner, Yu. Grin, *Chem. Eur. J.* **2009**, *15*, 1673–1684.

[32] S. E. Ashbrook, L. Le Pollès, R. Gautier, C. J. Pickard, R. I. Walton, *Phys. Chem. Chem. Phys.* **2006**, *8*, 3423–3431.

[33] S. J. Clark, M. D. Segall, C. J. Pickard, P. J. Hasnip, M. J. Probert, K. Refson, M. C. Payne, *Z. Kristallogr.* **2005**, *220*, 567–570.

[34] M. Profeta, F. Mauri, C. J. Pickard, *J. Am. Chem. Soc.* **2003**, *125*, 541–548.

[35] J. R. Yates, C. J. Pickard, F. Mauri, *Phys Rev. B* **2007**, *76*, 024401.

[36] D. Brinkmann, W. Freudenreich, J. Ross, *Solid State Commun.* **1978**, *28*, 233–237.

[37] S.-T. Kong, H. J. Deiseroth, C. Reiner, Ö. Gün, E. Neumann, C. Ritter, D. Zahn, *Chem. Eur. J.* **2009**, in press.

[38] O. Pecher, S.-T. Kong, C. Reiner, H. J. Deiseroth, F. Haarmann, D. Zahn, *Chem. Eur. J.* **2009**, submitted.

[39] D. Trots, A. Senyshyn, D. A. Mikhailova, T. Vad, H. Fueß, *J. Phys.: Condens. Matter* **20** (2008) 455204.

[40] D. A. Keen, *J. Phys.: Condens. Matter* **2002**, *14*, R819-R857.

[41] R. Jacobson, Program REQAB, unpublished.

[42] M. Knapp, V. Joco, C. Baehtz, H. H. Brecht, A. Berghaeuser, H. Ehrenberg, H. von Seggern, H. Fueß, *Nuclear Instruments and Methods in Physics Research A* **2004**, *521*, 565–570.

[43] T. Roisnel, J. Rodriguez-Carvajal, WINPLOTR, Version May 2000, *Materials Science Forum*, Proceedings of the 7th European Powder Diffraction Conference 2000, Barcelona, Spain, 188. J. Rodriguez-Carjaval, FULLPROF.2K, Version 1.6; **2000**, Laboratoire Léon Brillouin: 2000, in: Abstract of Satellite Meeting on Powder Diffraction, Congress of the International Union of Crystallography, Toulouse, France, **1990**, 127.

[44] G. M. Sheldrick, SHELXL-97-2, Program for the Refinement of Crystal Structures, Universität Göttingen, Göttingen, Germany, 1997.

[45] M. Bak, J. T. Rasmussen, N. Ch. Nielsen, *J. Magn. Reson.* **2000**, *147*, 296–330.

[46] R. K. Harris, E. D. Becker, *J. Magn. Reson.* **2002**, *156*, 323–326.

[47] C. J. Pickard, F. Mauri, *Phys. Rev. B* **2001**, *63*, 245101.

[48] H. M. Petrilli, P. E. Blöchl, P. Blaha, K. Schwarz, *Phys. Rev. B* **1998**, *57*, 14690–14697.

[49] J. P. Perdew, K. Burke, M. Ernzerhof, *Phys. Rev. Lett.* **1996**, *77*, 3865–3868.

Received: ((will be filled in by the editorial staff))
Published online: ((will be filled in by the editorial staff))

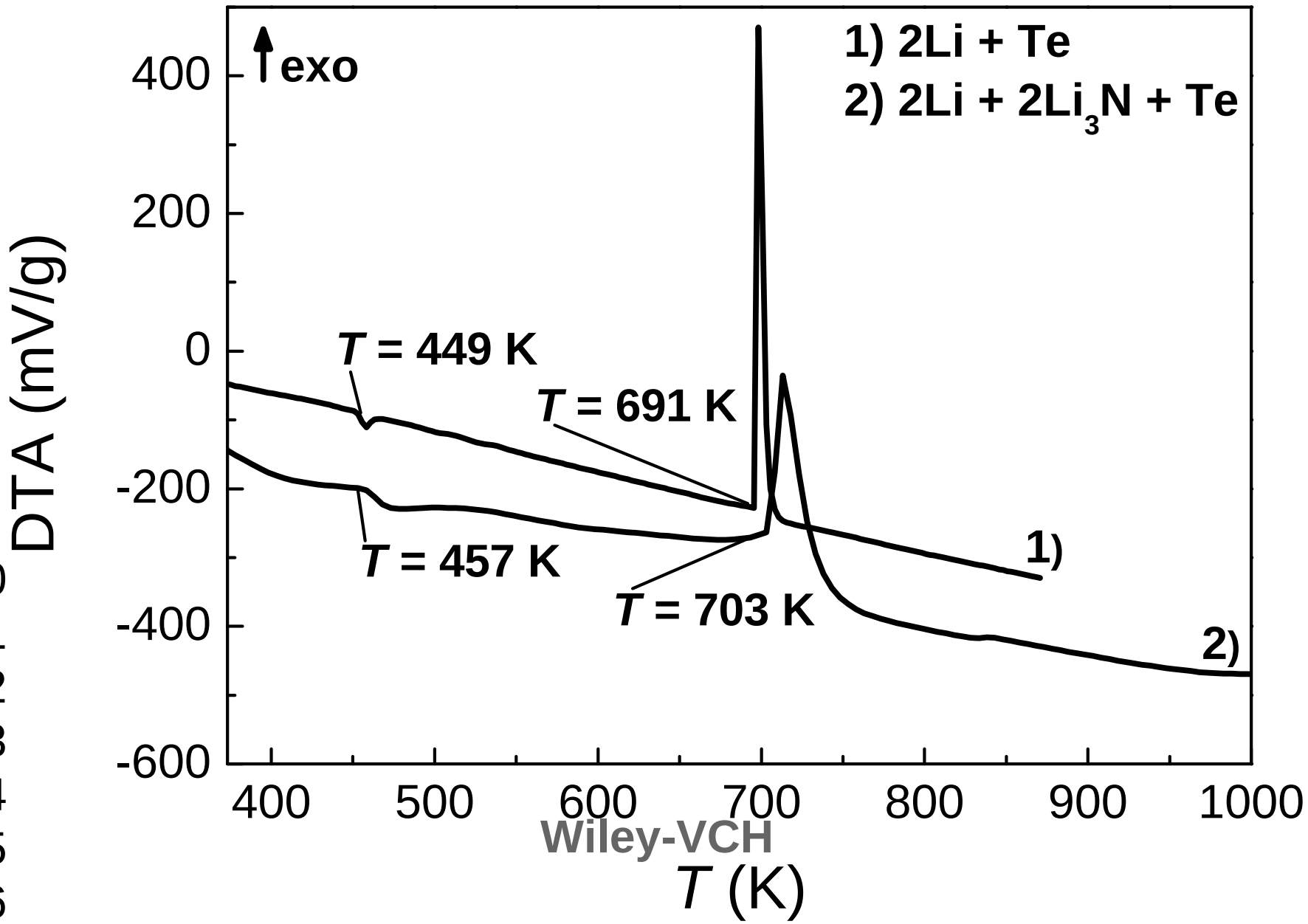
exo
1) 2Li + Te
2) 2Li + 2Li3N + Te
T = 449 K
T = 691 K
T = 457 K
T = 703 K
1)
2)
DTA (mV/g)
T (K)
400
200
0
-200
-400
-600
400
500
600
700
800
900
1000

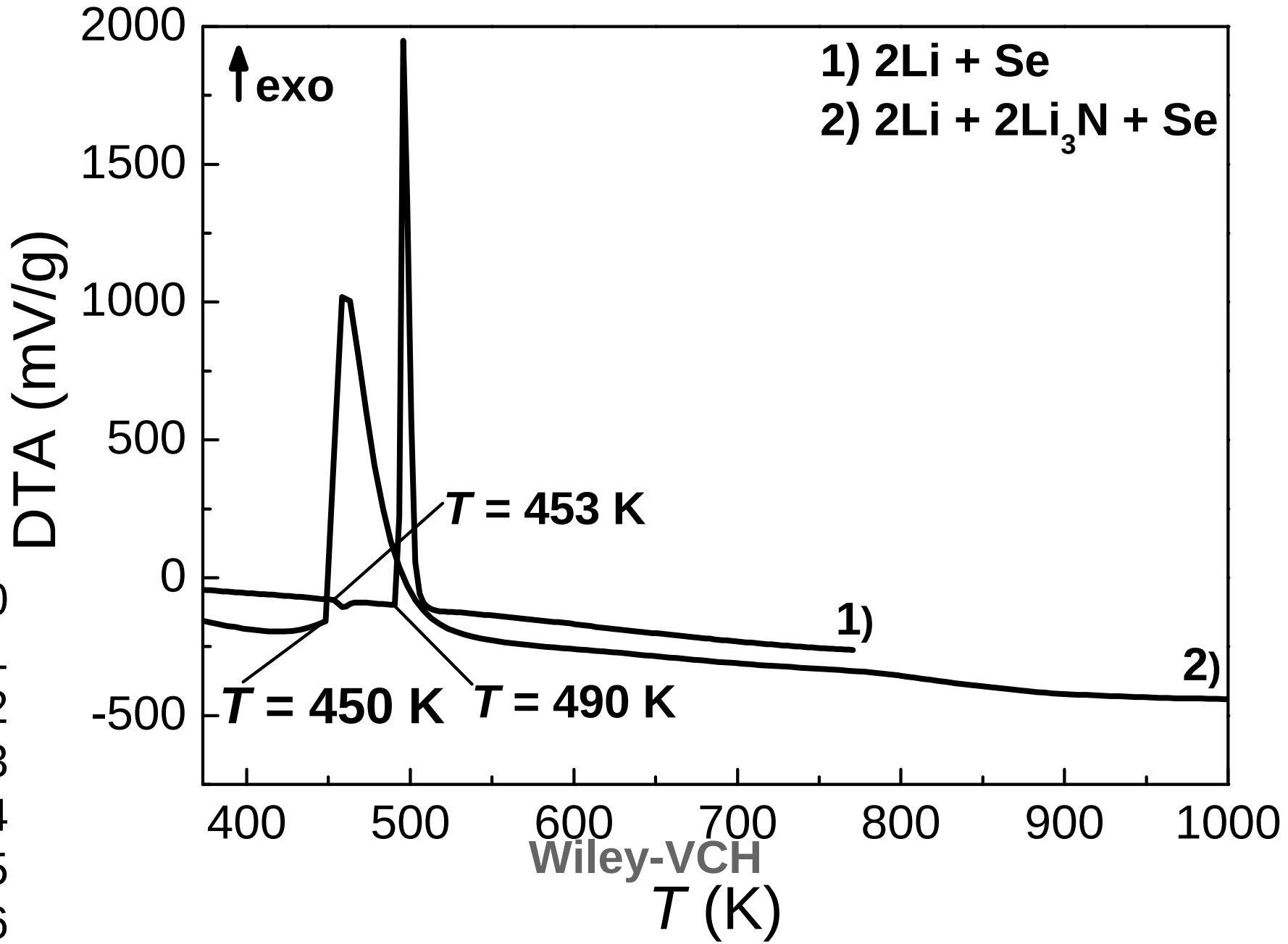
exo
1) 2Li + Se
2) 2Li + 2Li3N + Se
T = 453 K
T = 450 K
T = 490 K
1)
2)
DTA (mV/g)
T (K)
2000
1500
1000
500
0
-500
400
500
600
700
800
900
1000

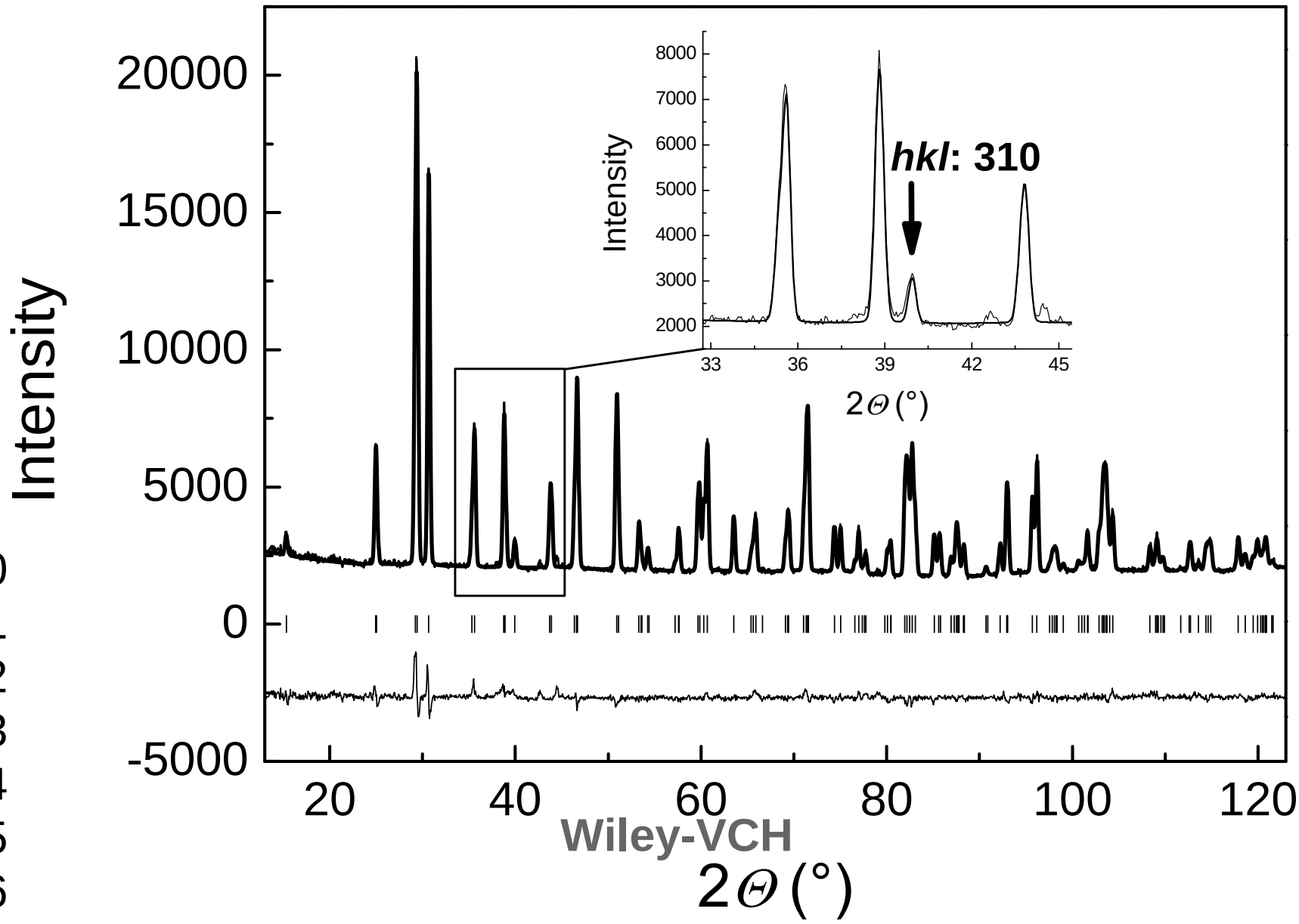
Intensity
20000
15000
10000
5000
0
-5000
20
40
60
80
100
120
2Θ (°)
Intensity
8000
7000
6000
5000
4000
3000
2000
33
36
39
42
45
2Θ (°)
hkl: 310

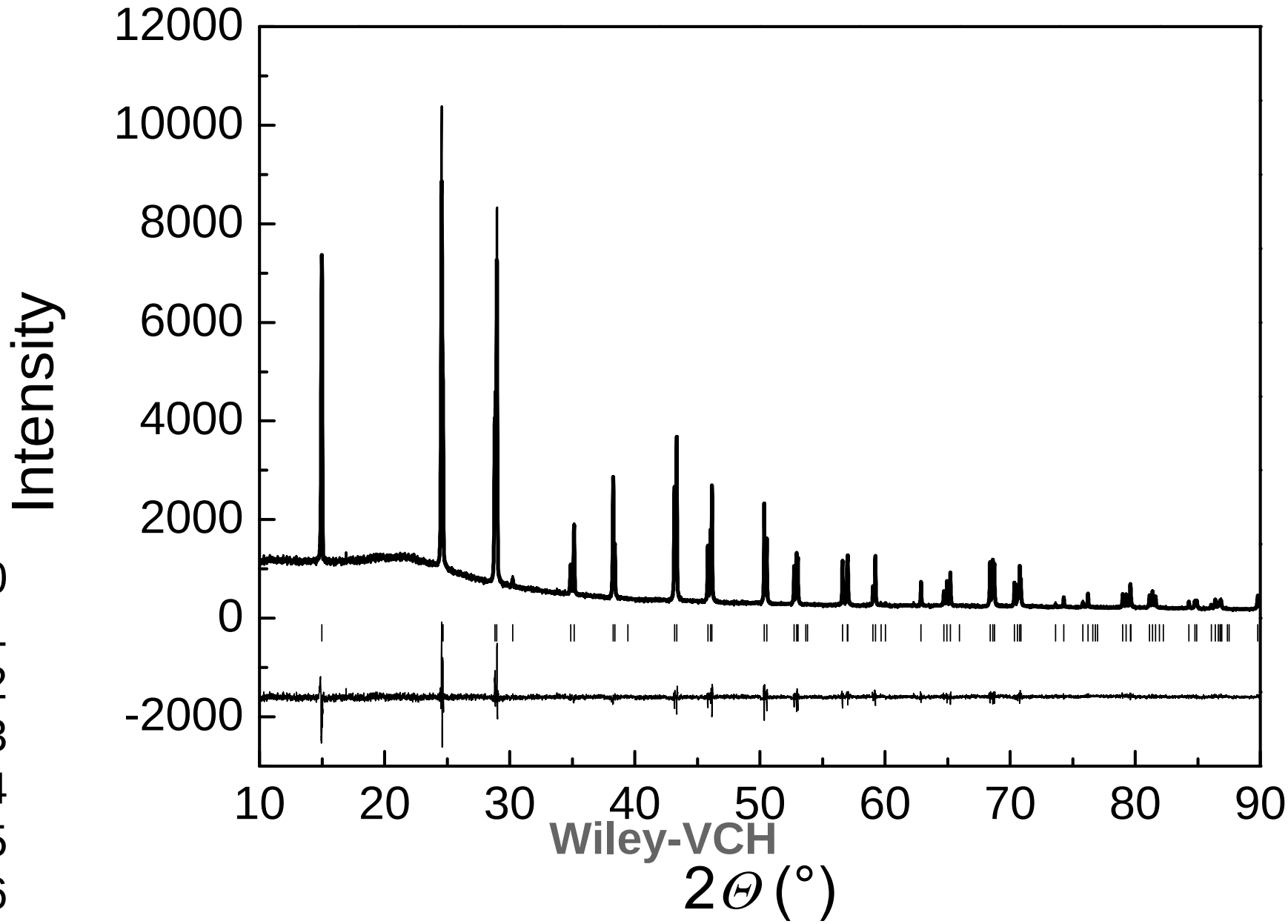
12000
10000
8000
6000
4000
2000
0
-2000
Intensity
10
20
30
40
50
60
70
80
90
2Θ (°)

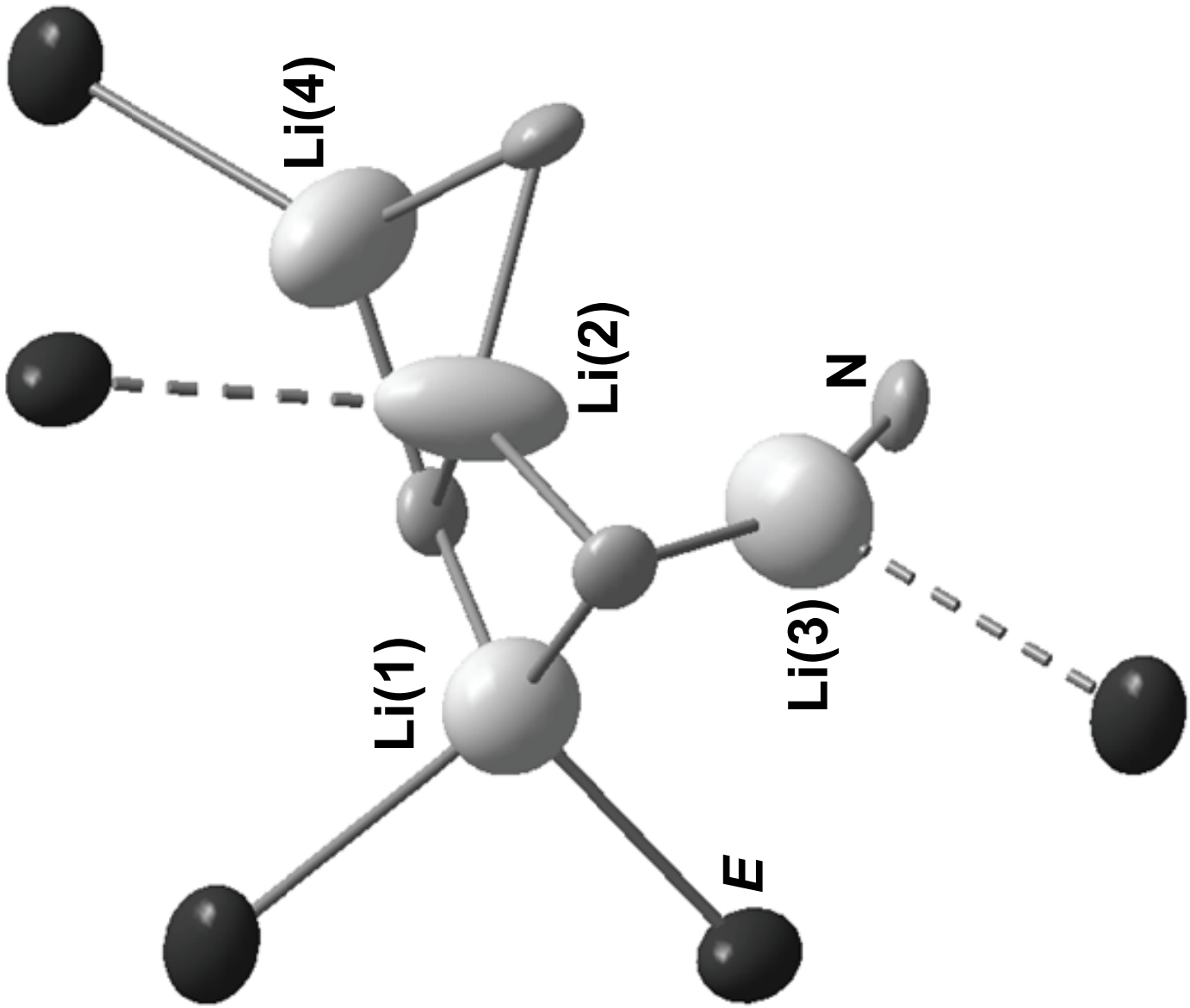
Li(4)
Li(2)
N
Li(3)
Li(1)
E

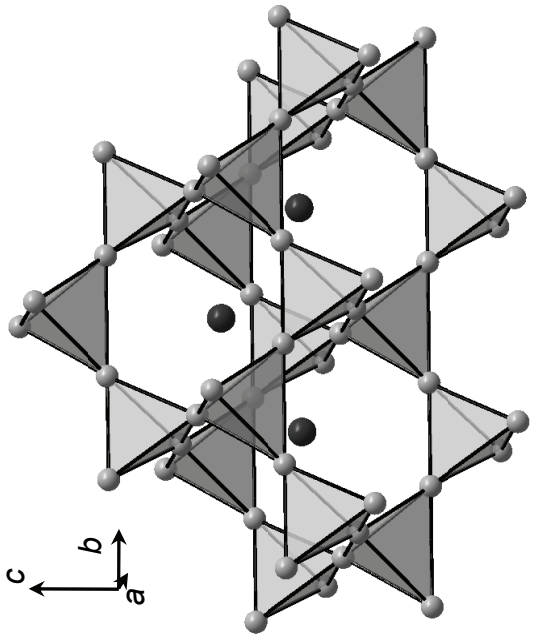
b
c
a

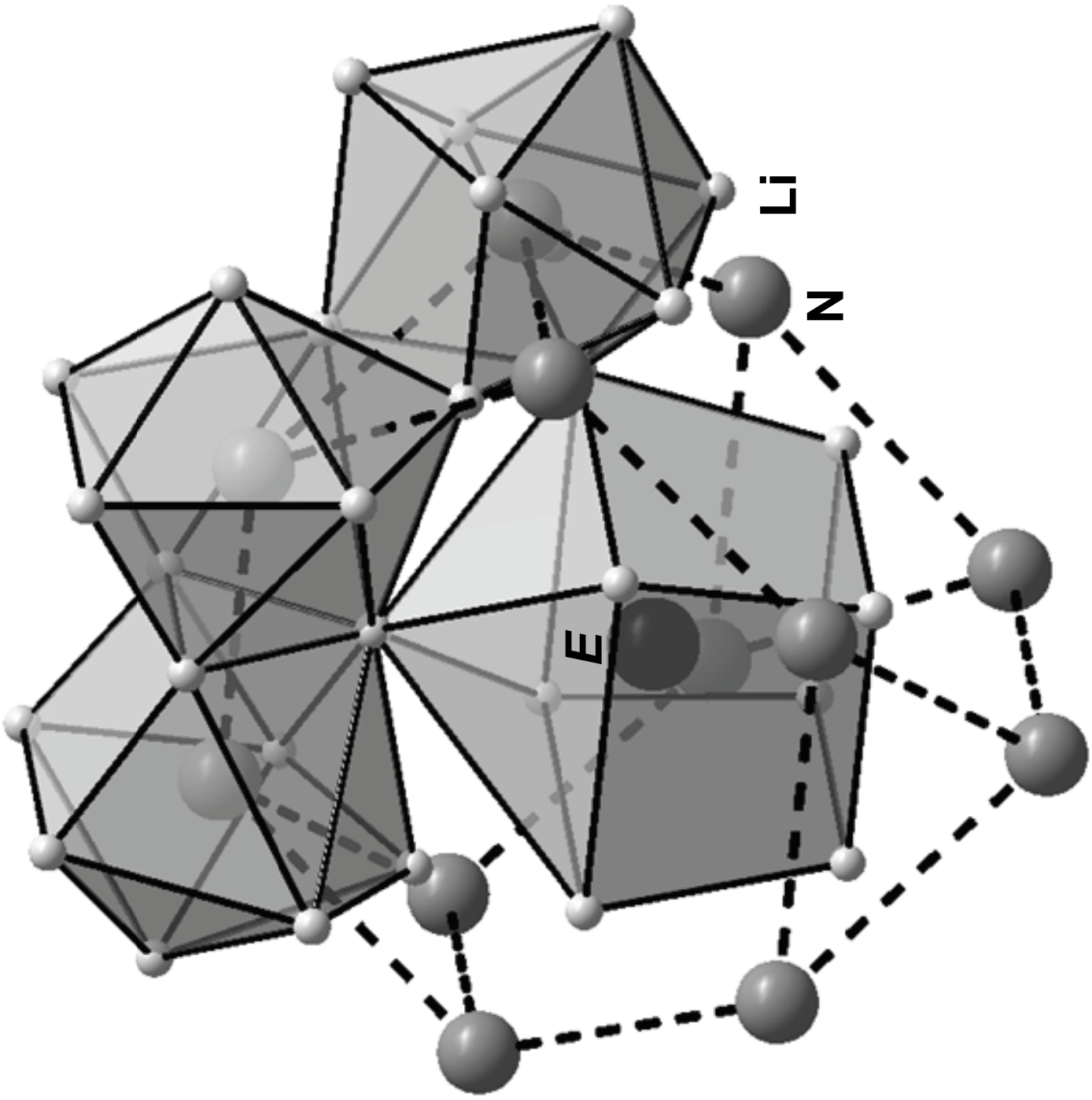
Li
N
E

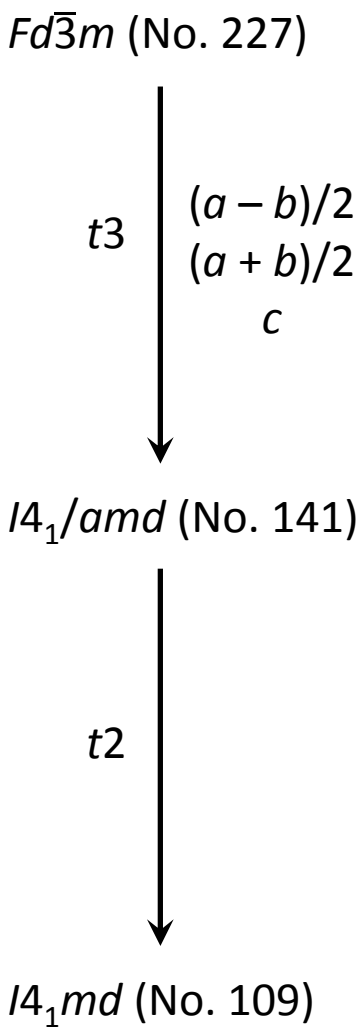

Mg: 8*a*	Cu: 16*d*
$\bar{4}3m$	$.\bar{3}m$
0	5/8
0	5/8
0	5/8

$(x - y)$, $(x + y)$, z

E: 4*a*	N: 8*d*
4*m*2	.2/*m*.
0	0
0	1/4
0	5/8

E: 4*a*	N: 8*d*
2*mm*.	.*m*.
0	1/2
0	$-y + 1/2$
Z	$z + 1/2$

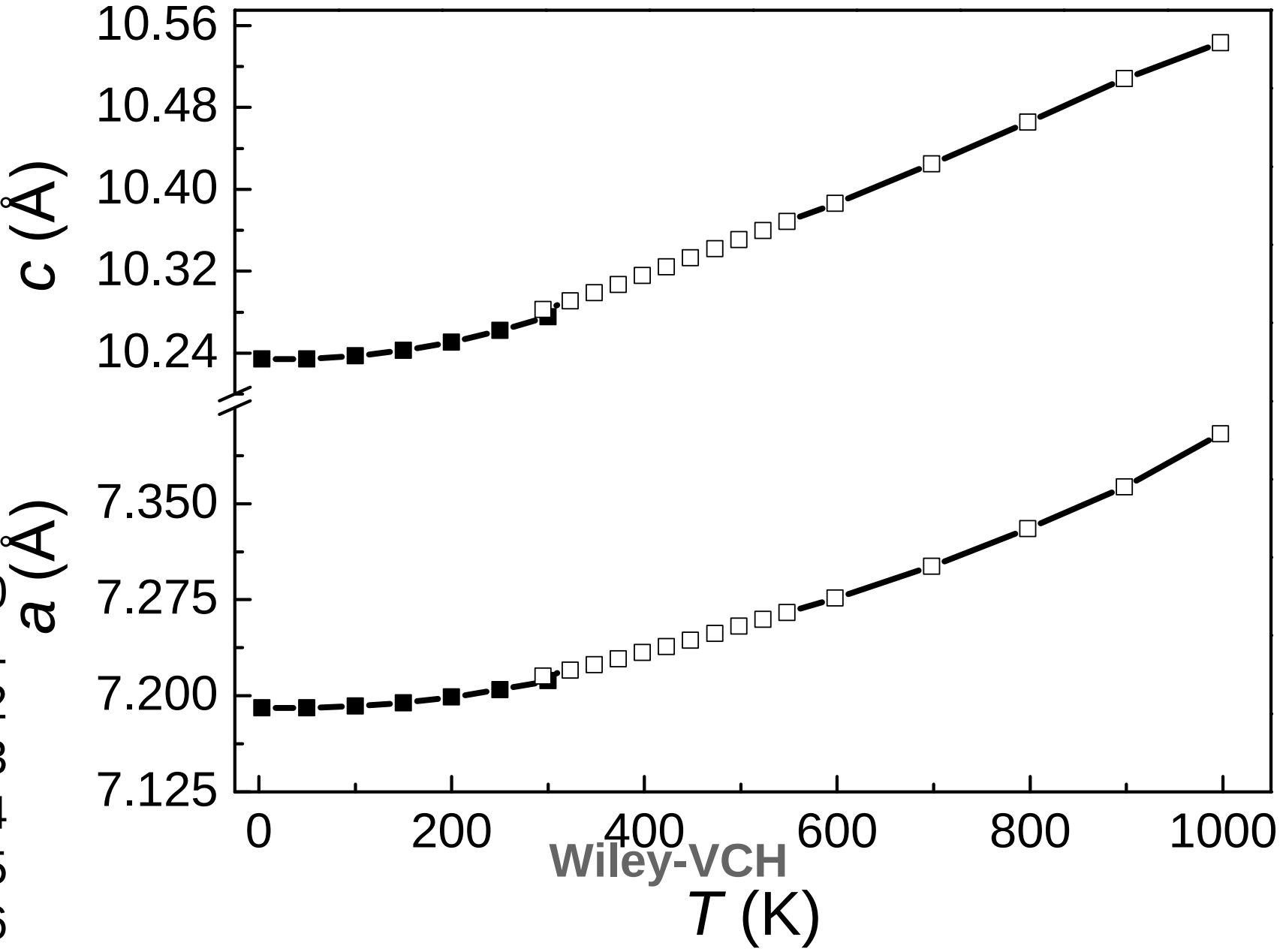
10.56
10.48
10.40
10.32
10.24
c (Å)
7.350
7.275
7.200
7.125
a (Å)
0
200
400
600
800
1000
T (K)

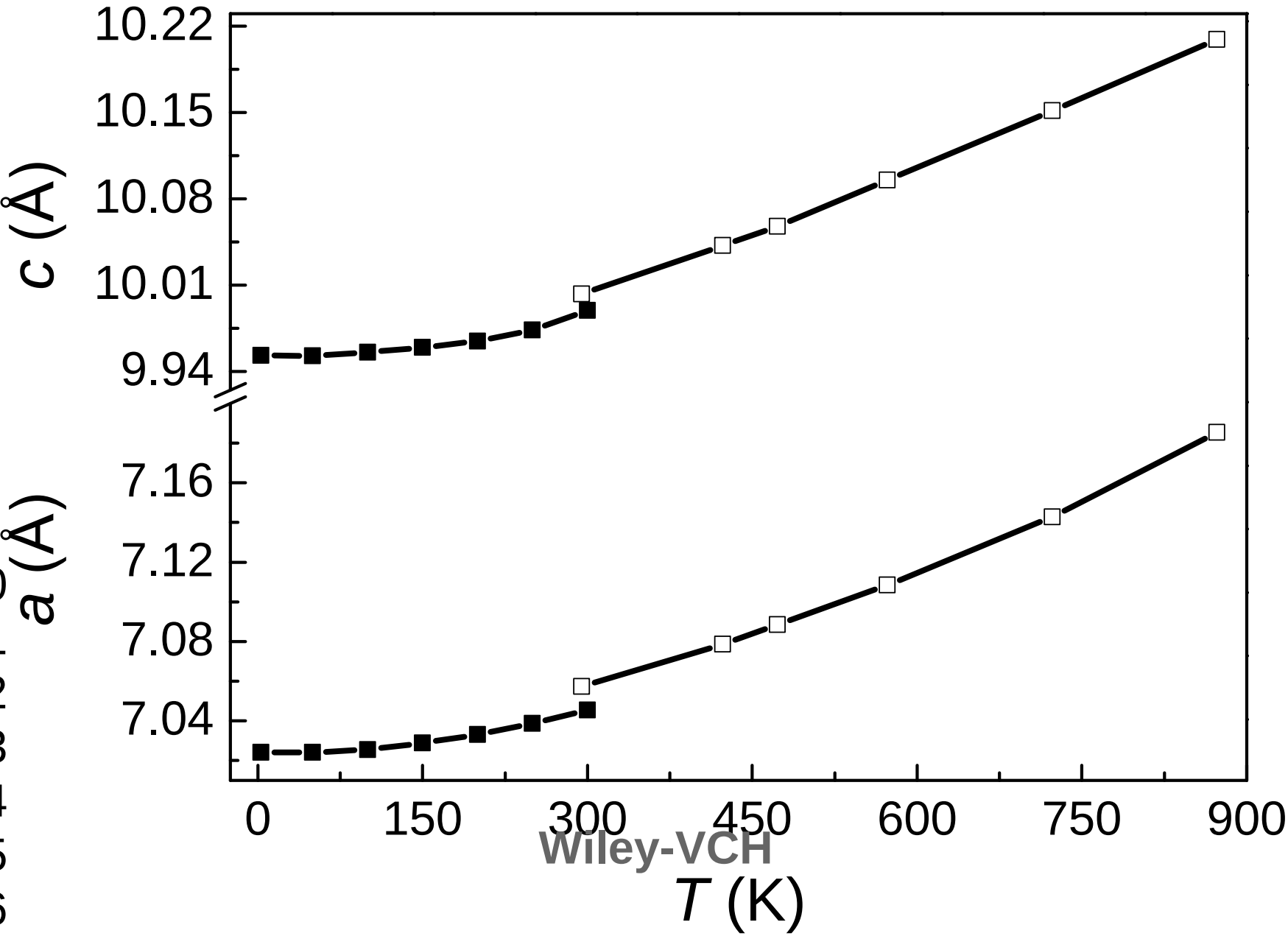
10.22
10.15
10.08
10.01
9.94
c (Å)
7.16
7.12
7.08
7.04
a (Å)
0
150
300
450
600
750
900
T (K)

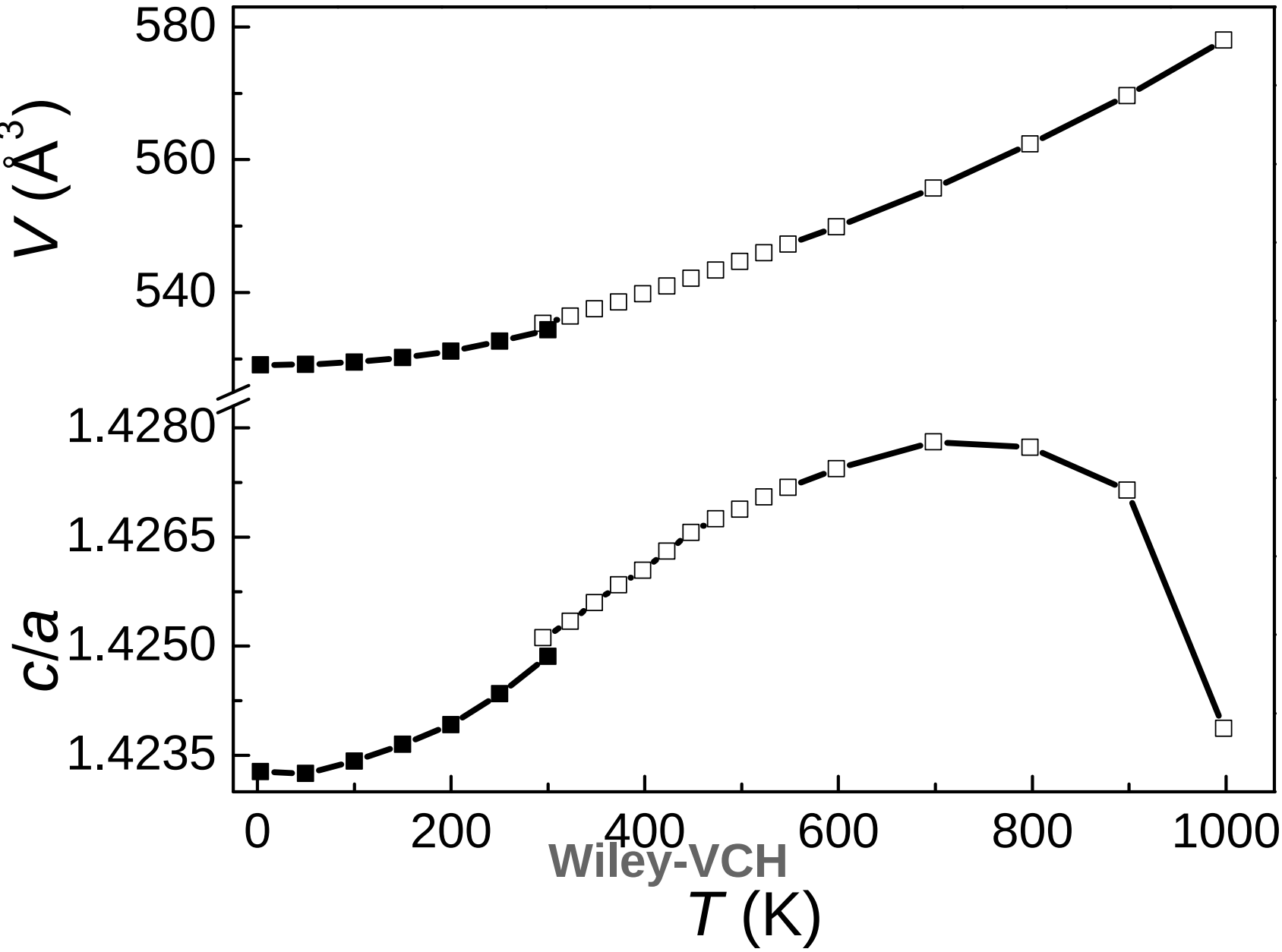
580
560
540
1.4280
1.4265
1.4250
1.4235
V (Å3)
c/a
0
200
400
600
800
1000
T (K)

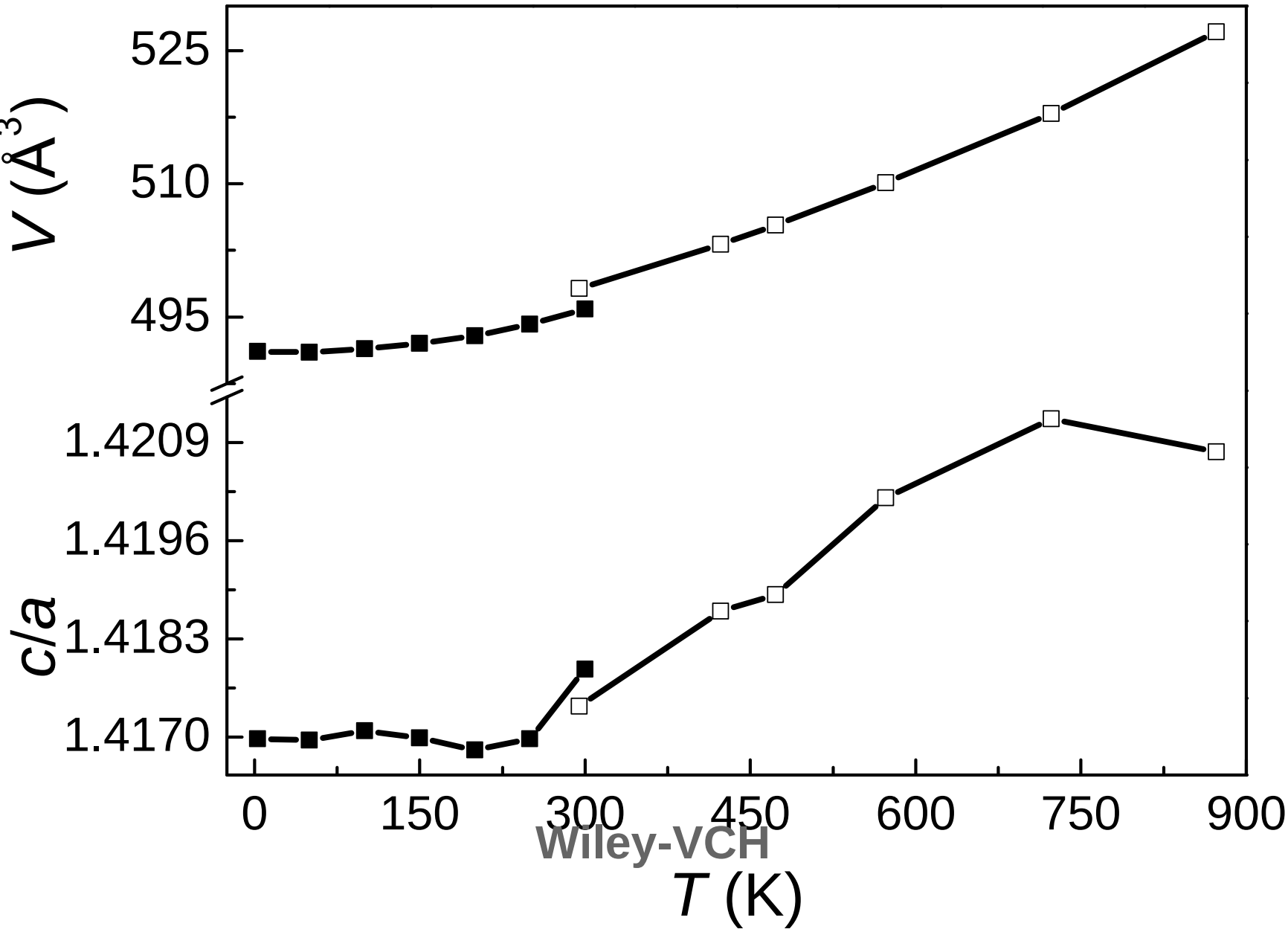
525
510
495
V (Å3)
1.4209
1.4196
1.4183
1.4170
c/a
0
150
300
450
600
750
900
T (K)

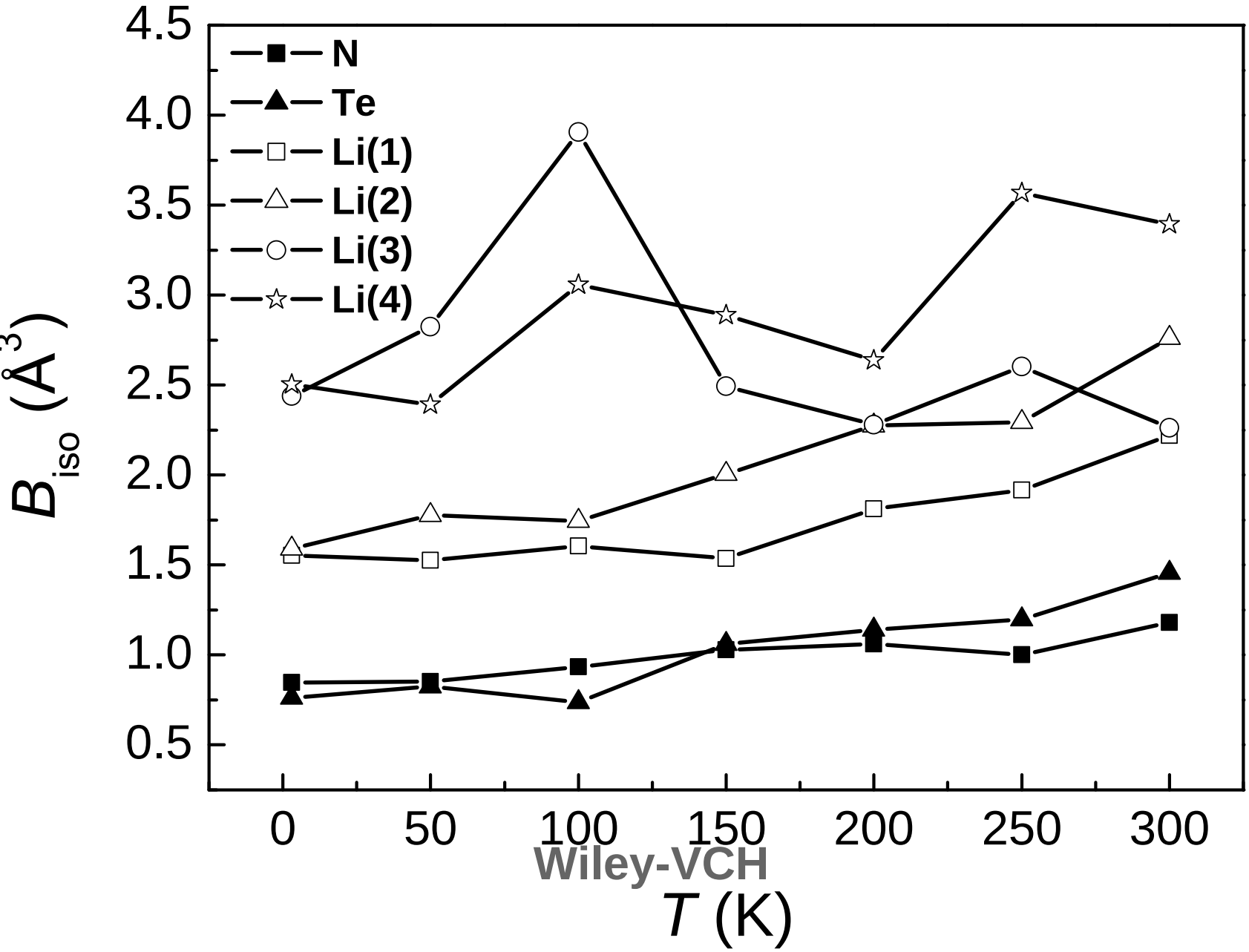
N
Te
Li(1)
Li(2)
Li(3)
Li(4)
B_{iso} (Å^3)
4.5
4.0
3.5
3.0
2.5
2.0
1.5
1.0
0.5
0
50
100
150
200
250
300
T (K)

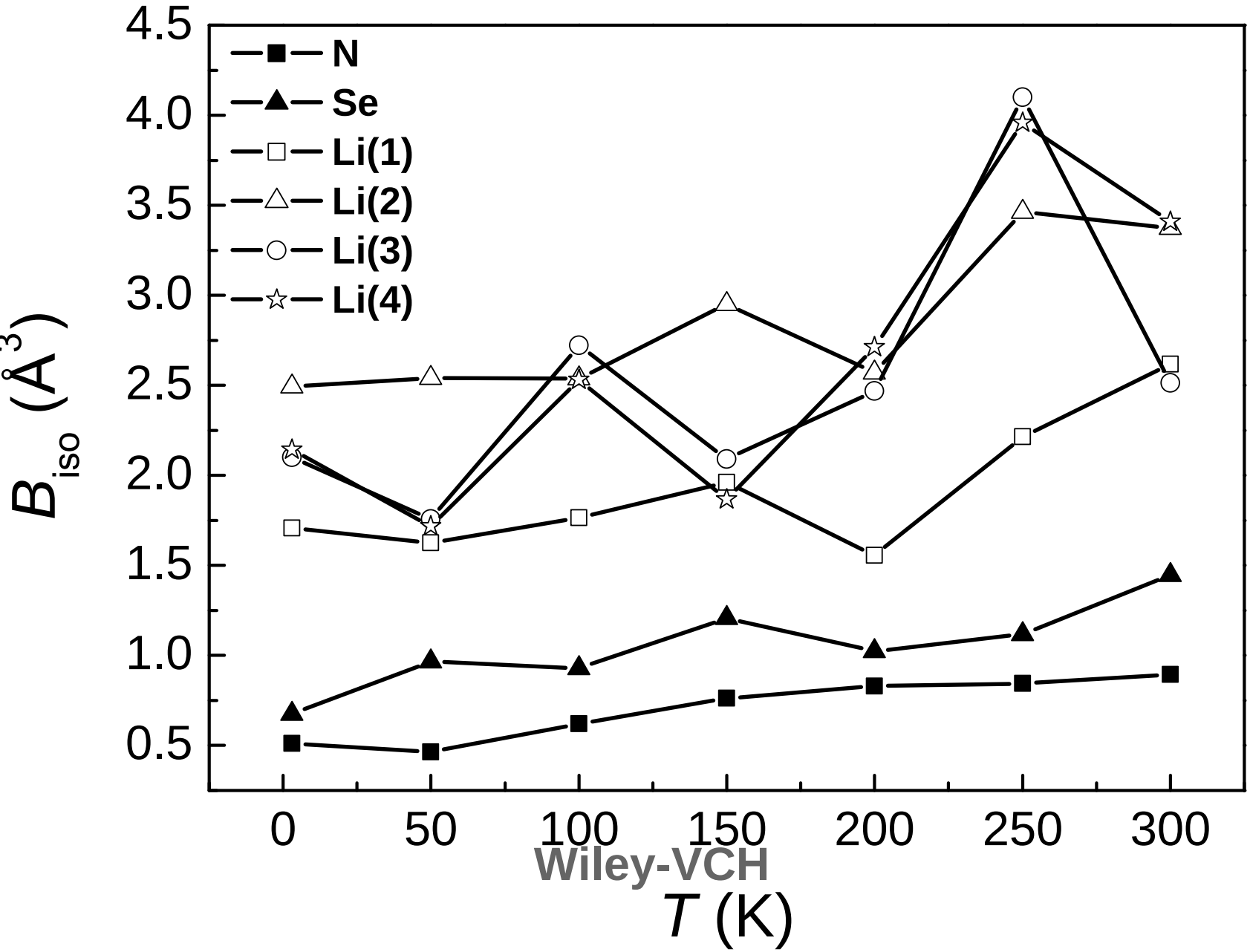
N
Se
Li(1)
Li(2)
Li(3)
Li(4)
B_{iso} (Å^3)
T (K)
4.5
4.0
3.5
3.0
2.5
2.0
1.5
1.0
0.5
0
50
100
150
200
250
300

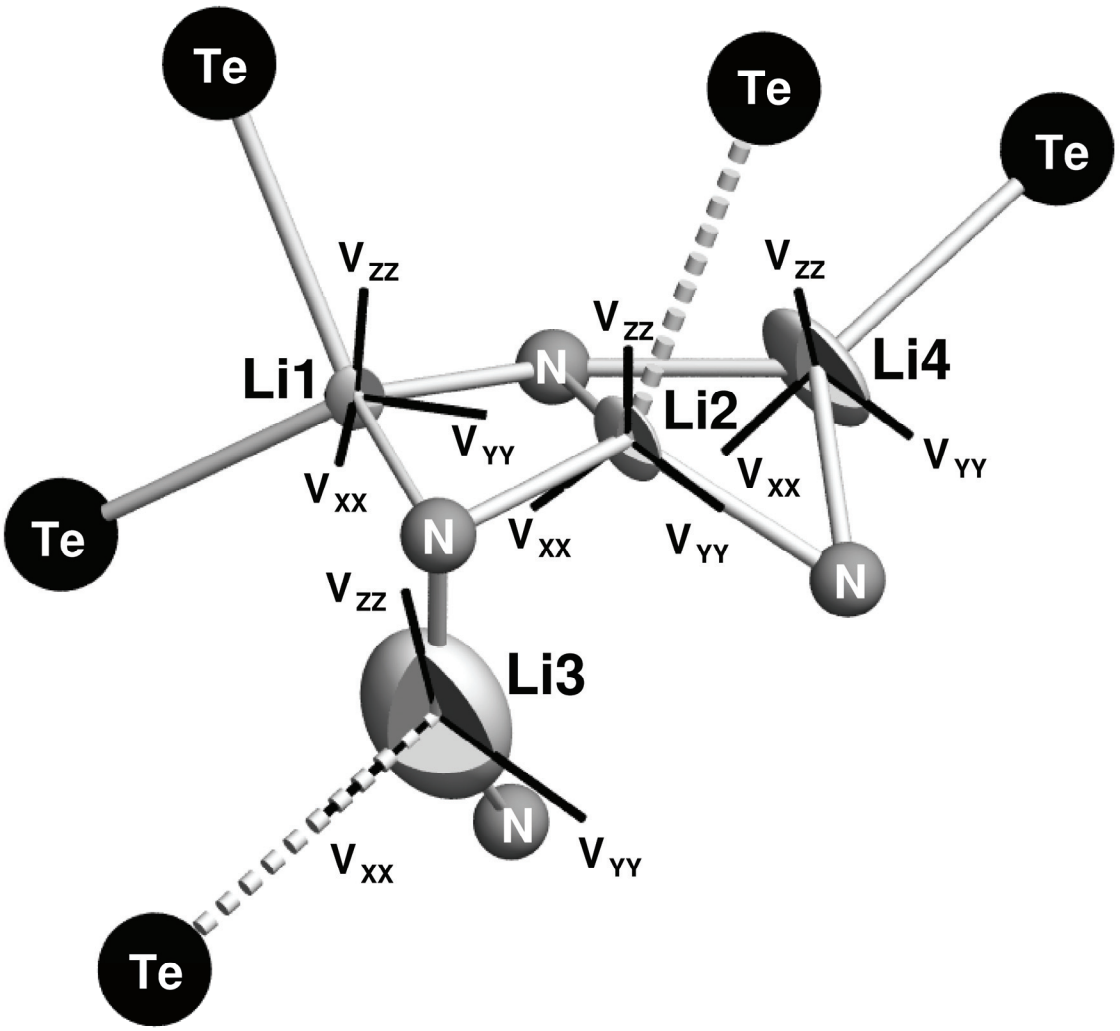
Te
Te
Te
Te
Li1
Li2
Li3
Li4
N
N
N
N
V zz
V zz
V zz
V zz
V xx
V xx
V xx
V xx
V yy
V yy
V yy
V yy

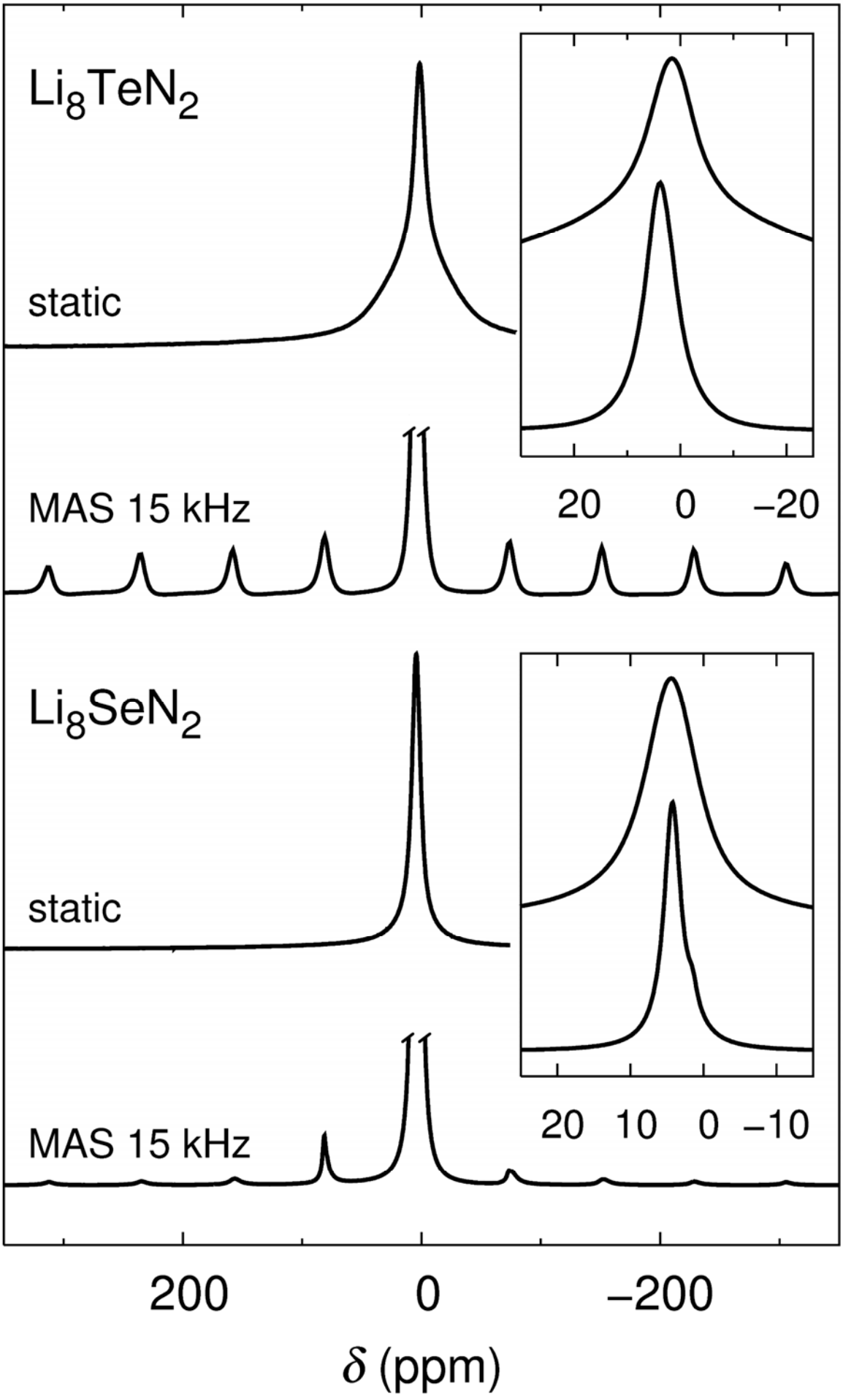
Li8TeN2
static
MAS 15 kHz
20 0 –20
Li8SeN2
static
MAS 15 kHz
20 10 0 –10
200 0 –200
δ (ppm)

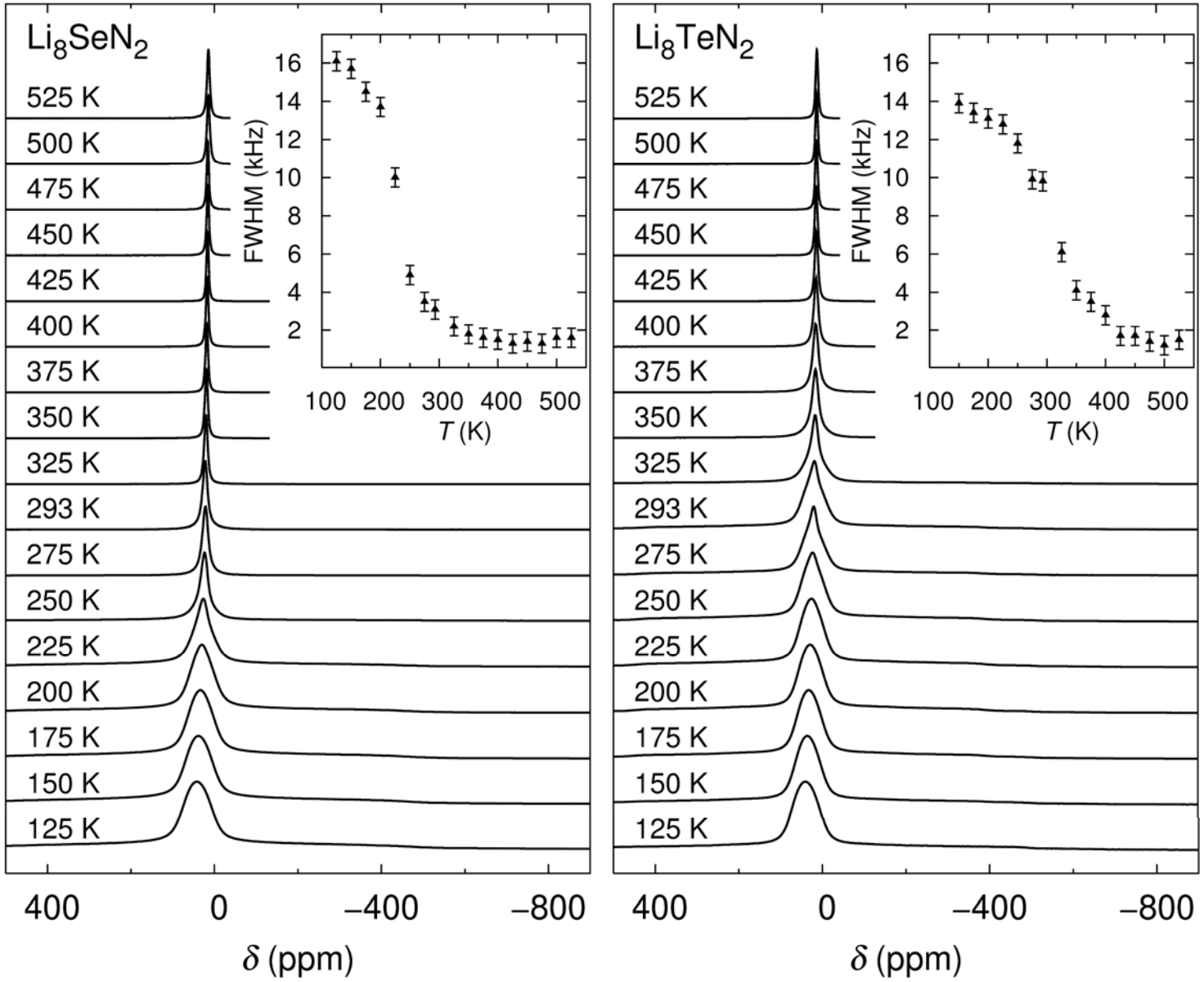
Li8SeN2
525 K
500 K
475 K
450 K
425 K
400 K
375 K
350 K
325 K
293 K
275 K
250 K
225 K
200 K
175 K
150 K
125 K
FWHM (kHz)
16
14
12
10
8
6
4
2
100 200 300 400 500
T (K)
400 0 −400 −800
δ (ppm)
Li8TeN2
525 K
500 K
475 K
450 K
425 K
400 K
375 K
350 K
325 K
293 K
275 K
250 K
225 K
200 K
175 K
150 K
125 K
FWHM (kHz)
16
14
12
10
8
6
4
2
100 200 300 400 500
T (K)
400 0 −400 −800
δ (ppm)

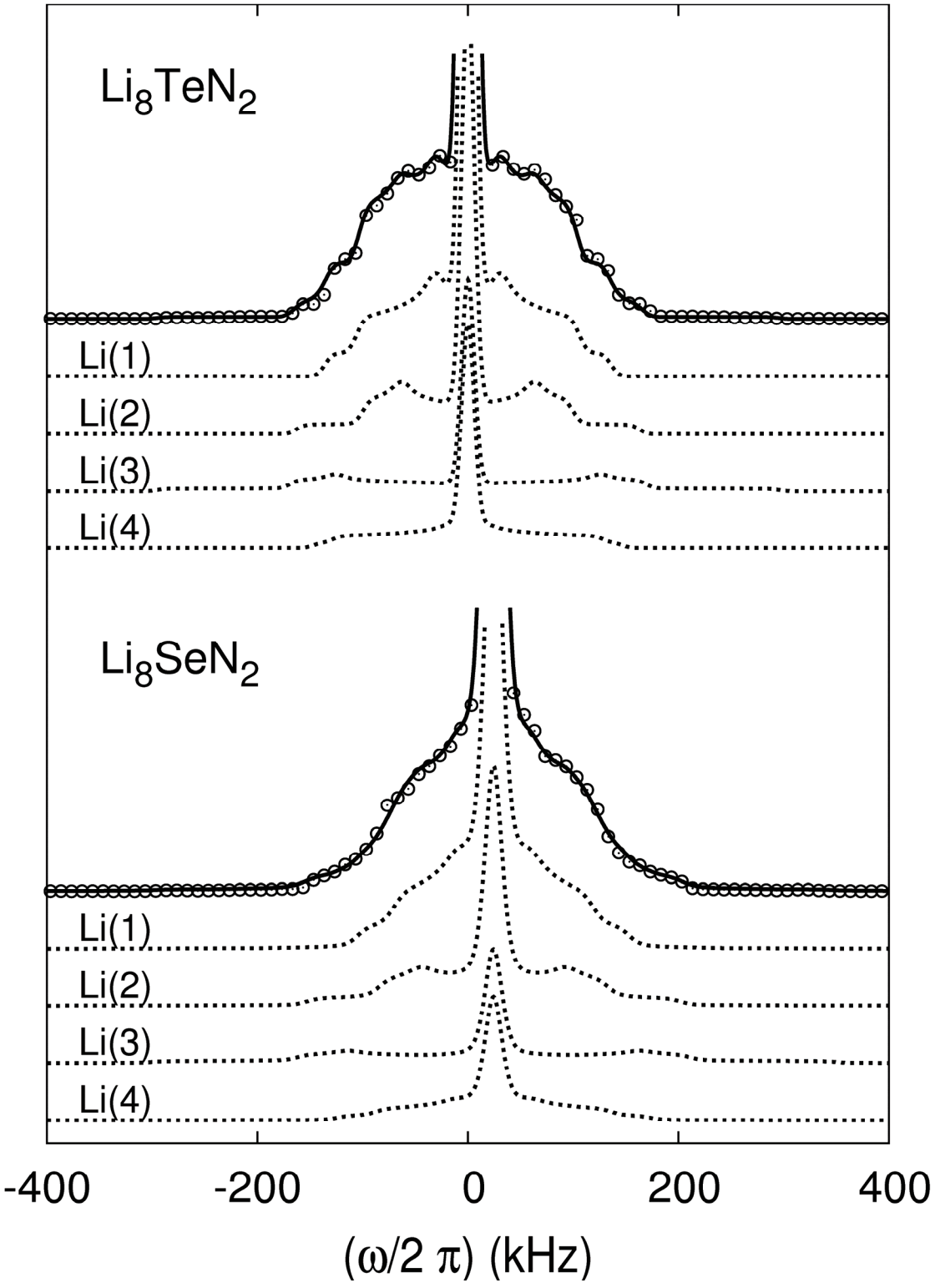
Li8TeN2
Li(1)
Li(2)
Li(3)
Li(4)
Li8SeN2
Li(1)
Li(2)
Li(3)
Li(4)
-400
-200
0
200
400
(ω/2 π) (kHz)